4-2014

Seasonal dynamics of a suburban energy balance in Phoenix, Arizona

Winston T. L. CHOW
Singapore Management University, winstonchow@smu.edu.sg

Thomas J. VOLO

Enrique R. VIVONI

G. Darrel JENERETTE

Benjamin L. RUDDELL

Citation

RMetS

Royal Meteorological Society

Seasonal dynamics of a suburban energy balance in Phoenix, Arizona

Winston T. L. Chow,[a,b]* Thomas J. Volo,[c] Enrique R. Vivoni,[c,d] G. Darrel Jenerette[e] and Benjamin L. Ruddell[b]

[a] *Department of Geography, National University of Singapore, Singapore*
[b] *Department of Engineering, Arizona State University, Mesa, AZ, USA*
[c] *School of Sustainable Engineering and the Built Environment, Arizona State University, Tempe, AZ, USA*
[d] *School of Earth and Space Exploration, Arizona State University, Tempe, AZ, USA*
[e] *Department of Botany & Plant Sciences, University of California – Riverside, CA, USA*

ABSTRACT: Observations of local-scale urban surface energy balance (SEB), which include fluxes of net all-wave radiation ($Q*$), and eddy covariance measurements of sensible (Q_H) and latent heat (Q_E) were collected in an arid Phoenix, AZ suburb from January to December 2012. We studied diurnal variations in SEB partitioning over four distinct seasons: winter, equinoxes, and summer; the latter period is further subdivided into (1) months prior to and (2) months occurring during the North American Monsoon. Largest flux densities were observed in summer, with most available energy partitioned into Q_H. Much less energy is partitioned into Q_E, but this term is strongly affected by monsoonal precipitation, where greater-than-average Q_E can be discerned for several days after storm events. The presence of a positive daily flux residual (RES) [i.e. $Q* - (Q_H + Q_E)$] for most of the summer indicates that anthropogenic heat (Q_F) from residential cooling is likely a significant factor influencing SEB. Analysis of hourly ensemble SEB fluxes during all seasons also indicates that RES is largest in the morning, but Q_H dominates in the afternoon. Results of SEB trends and magnitudes from Phoenix were also compared with other urban sites, especially in (sub)tropical cities. When normalized with net radiation terms, a consistent diurnal hysteresis between ensemble Q_H and RES occurs, suggesting a robust parameterization of this relationship for model development during clear-sky conditions. SEB dynamics also appear to be affected by local surface characteristics, with regular nocturnal negative Q_H associated with a high urban sky-view factor. Measured Q_E fluxes during dry seasons were larger than expected based on the small proportion of irrigated plan area vegetated surfaces. A probable explanation could be an enhanced micro-scale advective forcing of evapotranspiration arising from leading-edge effects over patchy residential lawns, which has possible implications for modelling evapotranspiration in hot arid cities.

KEY WORDS   surface energy balance; urban climate; evaporation

Received 19 December 2012; Revised 5 January 2014; Accepted 9 January 2014

1. Introduction

The urbanization process results in distinct alterations of the near surface atmosphere across multiple spatial and temporal scales (Oke, 1987). Manifestations of these include the urban heat island (UHI) and adverse air quality. While numerous studies document these phenomena in cities worldwide through descriptive observations of climate variables (e.g. urban temperature, humidity, precipitation, etc.) [see Arnfield (2003) for a review], research into understanding surface-atmosphere exchanges of momentum, heat, water and other gases is also essential so as to advance the physical knowledge of urban climates. This knowledge is essential for modelling and management of the urban climate, among

other applications (Grimmond *et al.*, 2010a; Pataki *et al.*, 2011). The surface-atmosphere energy exchanges can be measured empirically through the urban surface energy balance (SEB) of a near-surface active layer (or volume) between mean building roof height and the surface (Oke, 1988). This can be expressed as:

$$Q* + Q_F = Q_H + Q_E + \Delta Q_S + \Delta Q_A \left(\text{W m}^{-2} \right) \quad (1)$$

with

$$Q* = (K_{inc} - K_{out}) + (L_{inc} - L_{out}) \quad (2)$$

where $Q*$ is the net all-wave radiation; Q_F is the anthropogenic heat flux density (e.g. Sailor, 2011); Q_H and Q_E refer to the turbulent sensible and latent heat flux exchange between the urban surface and the atmosphere, respectively, which are usually an output for the urban surface during daytime, or input for the atmosphere; ΔQ_S and ΔQ_A are the net changes of heat storage and advection into the urban system; K_{inc} (L_{inc}) and K_{out} (L_{out}) are

*Correspondence to: W. T. L. Chow, Department of Geography, National University of Singapore, 1 Arts Link, AS2, #04-32, Kent Ridge, Singapore 119260, Singapore. E-mail: winstonchow@nus.edu.sg

the incoming and outgoing short-wave (long-wave) radiation flux densities measured above the urban canopy. Such investigation, especially over different spatial and temporal contexts, is also important for both expanding our existing scientific knowledge of current urban meteorology (Grimmond *et al.*, 2010b), and for the application of this knowledge towards architectural design and sustainable urban planning policies (Mills *et al.*, 2010).

Historically, urban SEB measurements have utilized point observations from flux towers with aerodynamic profile or eddy covariance (EC) methods enabling temporal analyses of local-scale ($\sim 10^4 - 10^6$ m^2) fluxes, as well as from aircraft and/or remote sensing platforms allowing for larger spatial averages of urban flux densities. Many recent studies used the EC technique to directly measure urban SEB fluxes (Grimmond and Christen, 2012); although these were mostly conducted over suburban residential land use/land cover (LULC). Most urban EC studies were concentrated in temperate or mid- and high-latitude cities, such as in Basel (Christen and Vogt, 2004; Rotach *et al.*, 2005), Christchurch (Spronken-Smith, 2002; Spronken-Smith *et al.*, 2006), Helsinki (Vesala *et al.*, 2008), Lodz (Offerle *et al.*, 2005a, 2006), London (Kotthaus and Grimmond, 2012), Marseille (Grimmond *et al.*, 2004), Melbourne (Coutts *et al.*, 2007), Tokyo (Moriwaki and Kanda, 2004) and Vancouver (Grimmond and Oke, 1999; Christen *et al.*, 2011). Urban SEB research within tropical and subtropical cities (i.e. sited within Köppen *A*, *B* or in some *H* climates), however, received disproportionately less attention in the studies published, as well as in duration of datasets and number of flux towers used in each city (Roth, 2007). Despite this bias, results from measurement campaigns undertaken in Cairo (Frey *et al.*, 2011), Mexico City (Oke *et al.*, 1992, 1999; Tejeda-Martinez and Jauregui, 2005), Mexicali (Garcia-Cueto *et al.*, 2003), Miami (Newton *et al.*, 2007), Ouagadougou (Offerle *et al.*, 2005b) and Tucson (Grimmond and Oke, 1995) have been important in broadening urban SEB knowledge across cities sited in different climates.

Urban energy exchanges are controlled by land surface characteristics (e.g. Oke, 2006), such as its cover (i.e. proportion of impervious *vs* pervious surfaces), structure (i.e. building-surface morphology such as aspect ratio and sky-view factor), fabric (i.e. proportion of different urban materials and their implicit thermal properties) and metabolism (i.e. anthropogenic emission of waste heat), all of which are important in determining the variation of SEB fluxes within cities. The importance of each urban SEB component is affected by its geographical location and associated synoptic climatology. For example, within cities located in tropical or subtropical areas subject to frequent and ample precipitation, the influence of copious surface and subsurface evapotranspiration into the urban atmosphere is critical in determining diurnal magnitudes of Q_E, often reducing ΔQ_S (Roth, 2007). Seasonal variations in precipitation regimes and insolation are also important in affecting energy partitioning between the

Q_H and Q_E, as seen in the significant variance in Bowen ratio ($\beta = Q_H / Q_E$) as a function of surface vegetation cover within a city (Loridan and Grimmond, 2012). These extant generalizations from numerous datasets are valuable for testing and improving urban climate models (Grimmond *et al.*, 2010b, 2011).

We present and analyse local-scale EC measurements collected during a calendar year (2012) over a suburban residential neighbourhood in the desert city of Phoenix, AZ. This site has operated since November 2011, as part of the Central Arizona-Phoenix Long-Term Ecological Research (CAP-LTER) project. The primary objective of this study is in determining the ensemble-averaged diurnal and seasonal dynamics of this system's SEB, with consideration for synoptic and regional weather (e.g. the onset of the North American summer monsoon). We examine trends of each radiative and turbulent flux with respect to net radiation between seasons, and also investigate the dynamics of the residual flux density measured at the site with respect to measured ground heat fluxes of bare soil and gravel and modelled stored heat flux from an empirically based urban climate model [Local-scale Urban Meteorological Parameterization Scheme; LUMPS (Loridan *et al.*, 2011)], which was configured for the study area. Comparisons with SEB fluxes measured in other cities of similar climates, along with its implications, will also be discussed.

2. Methodology

2.1. Study area and site LULC characteristics

A micrometeorological tower (site name: WPHX; 33.483847°N, 112.142609°W) was established at the suburb of Maryvale, in the city of Phoenix, AZ (Figure 1). Phoenix is, by population size, the sixth largest city in the United States (U.S. Census Bureau, 2010). It lies within a hot arid subtropical desert climate (Köppen climate classification *BWh*) with mild winters and extremely hot summers, where maximum daytime temperatures have reached 50 °C. During the summer months, the city's climate is also subject to the North American monsoon, which contributes nearly 40% of the total annual precipitation mostly through brief but intense thunderstorms (Adams and Comrie, 1997; Vivoni *et al.*, 2008). While there has been ample research into Phoenix's urban climate, in particular the UHI phenomenon within the boundaries of its metropolitan area (Fernando *et al.*, 2010; Jenerette *et al.*, 2011; Chow *et al.*, 2012; Lee *et al.*, 2012), much less focus has ensued on the fundamental surface energetics and its influence on near-surface climate. Several recent papers have modelled seasonal variations of urban SEB with LUMPS in Phoenix (Middel *et al.*, 2012a, 2012b), but there is an absence of long-term *in situ* observational platforms in the city.

The area around WPHX is suburban residential in land use, and its associated land cover largely consists of low-rise, single-story single-family residences of relatively small mean lot size (~ 700 m^2) (Chow and Brazel, 2012).
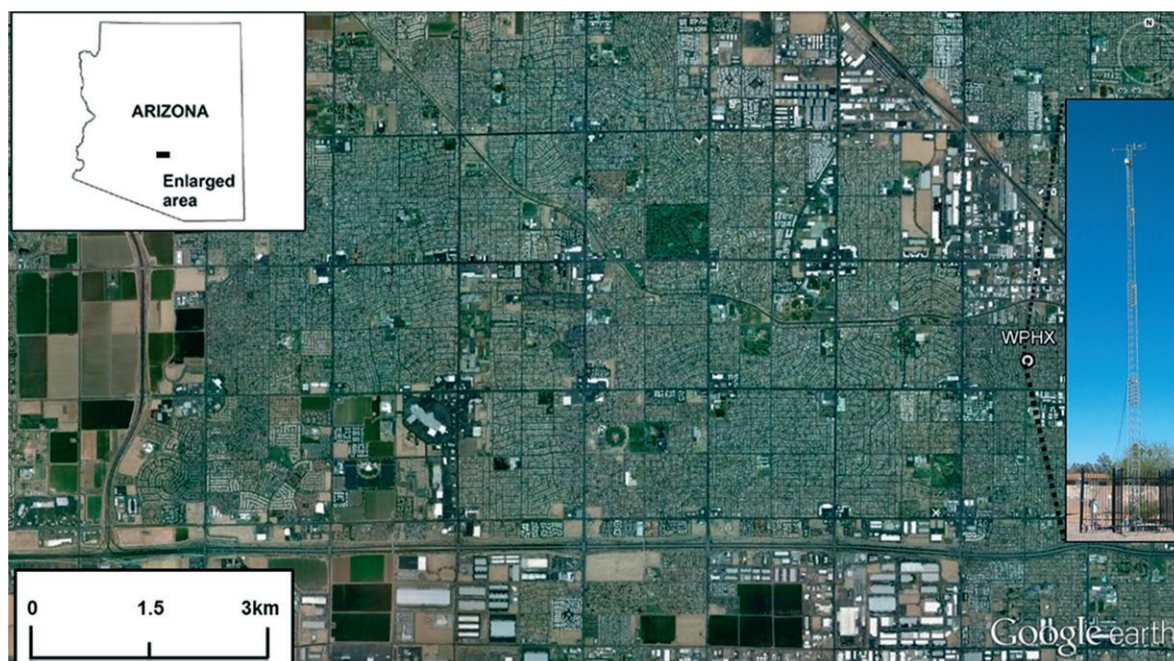
Figure 1. Location and image of WPHX flux tower sited in a residential suburban of Maryvale, in Phoenix, AZ. Note the extensive fetch of suburban residential land use and its associated land cover due west of the site. *Source*: Google Earth (basemap).

Each lot has small front and backyard spaces that generally total of $\sim$350 m^2. Landscaping in most yards in the neighbourhood was left unvegetated with bare, sandy soils that are characteristic of the surrounding desert, but about 20–25% of housing lots had Bermuda grass (*Cynodon dactylon*) yards. Also scattered infrequently throughout were landscaping trees typically used in metropolitan Phoenix [see Chow *et al.* (2011) for a list of species]. Landscaping conditions are mostly dry (xeric), as a large majority of residential lots do not possess automated watering systems (e.g. drip, flood or sprinkler irrigation). Instead, the use of garden hoses for *ad-hoc* lawn watering is prevalent. Swimming pools consisted of <1% of land cover and most residences leave them empty, even during the summer months. These residential houses were mostly developed between the late 1950s and early 1960s, and were constructed with light-coloured concrete block walls and dark-coloured asphalt shingle roofs. Measurements of estimated mean building roof heights (z_b), mean height to width/aspect ratio (H/W) and mean canyon sky-view factors (Ψ_S) of 4.5 m, 0.4 and 0.75, respectively, were taken during field surveys of the study area neighbourhood (Table 1). Together with the descriptive attributes of this site, these above measurements are typical properties associated with Local Climate Zone (LCZ) 6 as described by Stewart and Oke (2012).

To quantify the study area's general land cover characteristics, we obtained recent fine scale (2.4 m spatial resolution) Quickbird imagery of Phoenix compiled from 2006 to 2011. Land cover classification from the images was based on an object-based approach developed by Myint *et al.* (2011), which had an overall accuracy of 89.9% when compared to a stratified random sample of surface validation points in Phoenix. We subsequently

used ArcMap (version 10.1, ESRI Systems, Redlands, CA, USA) to analyse the land cover classification for an area of $\sim$1 km^2 immediately west of the tower site (Table 1; Figure 2). The analysis indicates impervious (48.4%) and sandy soil surfaces (36.8%) dominate the land cover of the residential area, with little grass and tree cover ($\sim$14.6%).

2.2. Site instrumentation, source area and operation

We employed an open-path EC setup to measure the study area's local-scale SEB for a total of 366 days during the calendar year 2012 [see Aubinet *et al.* (2012) for underlying EC theory and methodology]. The instruments are mounted near the apex of a TX-472 four-section lattice tower (US Tower Corporation Inc., Woodlake, CA, USA) at a height of 22.1 m AGL (above ground level) (Figure 1). This measurement height is approximately five times greater than z_b, so under most conditions the sensors are likely sited within the inertial sublayer, and thus measure a spatially averaged, integrated local-scale signal of turbulent fluxes (Oke, 2006). Three-dimensional wind velocities (u, v, w) and virtual sonic temperature (T_v) are measured by a CSAT3 sonic anemometer (Campbell Scientific Inc., Logan, UT, USA). Water vapour (q) and carbon dioxide (CO_2) fluxes are measured through a LI-7500 open-path infrared gas analyzer (Li-Cor Biosciences Inc., Lincoln, NE, USA), which was mounted $\sim$0.4 m away horizontally from the CSAT and tilted 30° from vertical to prevent moisture accumulation on the sensor. Every 6 months, the LI-7500 was subject to laboratory zero and spanning to ensure measurement accuracy with a LI-610 dew point generator (Li-Cor Biosciences Inc.). A HMP45AC (Vaisala Oyj, Helsinki, Finland) sensor within a radiation shield was also installed

Table 1. WPHX site metadata and associated LULC characteristics summarized as LCZ datasheet (Stewart and Oke, 2012).

LCZ definition	
Form	LCZ 6 (Open low-rise); flat terrain dominated by low-rise, single-family residential homes; mostly concrete and asphalt construction materials with much exposed bare, sandy soils and little grass and tree cover; little or no formal irrigation systems
Function/location	Suburban residential land use
Correspondence with Oke (2006) and Ellefsen (1990/1991)	UCZ 5 (medium development/low-density suburban); Do3 (open set house)
LCZ properties within study area (measured on-site, unless specified)	
Estimated mean Ψ_S	0.7–0.85
Estimated mean street canyon aspect ratio (H/W)	0.4
Mean roof height of buildings (z_b)	4.5 m
Mean typical tree height	4 m
Terrain roughness class[a]	6 (north, west and south of site); 5 (east of site)
Estimated thermal admittance (μ)[b]	1000–2200 J m^{-2} s$^{-1/2}$ K^{-1}
Mean albedo at solar noon[c]	0.168
Estimated hourly anthropogenic heat flux Q_F density[d]	25–36 W m^{-2} (daytime) 7–25 W m^{-2} (nighttime)
Land cover analysis of plan area around WPHX based on 2011 Quickbird image (2.4 m resolution) of 1 km^2	
Building surface fraction	26.42%
Roads/asphalt fraction	22.02%
Tree fraction	4.61%
Grass fraction	10.01%
Bare soil fraction	36.83%
Water/pool fraction	0.11%

[a]Refer to Oke (2006), Table 11.2. [b]Listed range of μ from Stewart and Oke (2012), with low (high) values representative of grass/soil (concrete, asphalt) surfaces. [c]Mean value observed from tower radiometer data. [d]Summer Q_F estimated from Figure 2 in Grossman-Clarke *et al.* (2005) through the inventory method of Sailor and Lu (2004).

adjacent to the CSAT3 and LI-7500 to sample ambient air temperature (T_a) and relative humidity (RH). These three sensors are mounted on a boom extending ∼1.2 m away from the tower, approximately four times the tower width at its narrowest section. The instruments are oriented to face west in the direction of greatest fetch (∼11 km) over the uniform suburban residential LULC, so as to minimize large variations of ΔQ_A that may influence other terms in Equation (1).

All incoming and outgoing radiation fluxes (K_{inc}, K_{out}, L_{inc}, L_{out}) are measured at the same height with a NR01 four-way net radiometer (Hukseflux, B.V., Delft, The Netherlands). Compared to several other net radiometers, the NR01 was tested to be the most accurate relative to a reference radiometer under all weather conditions (Blonquist *et al.*, 2009). Other relevant variables, which include precipitation, near-surface soil heat flux, soil temperature and moisture at various depths, were also measured either near or below the site surface through a suite of ground-based sensors (Table 2). Data from all instruments at the WPHX site are monitored through dataloggers mounted at the base of the tower (CR23X and CR1000, Campbell Scientific Inc.) that are powered through an outlet connected to an adjacent main power line.

The raw 10 Hz tower data were subsequently postprocessed through the EDIRE software platform (download available from http://www.geos.ed.ac.uk/abs/research/micromet/EdiRe/). Prior to analysis, the data were (1) signal de-spiked, with instantaneous values ±4σ during mean 30-min measurement periods being removed iteratively prior to subsequent corrections, with no data gap filling; (2) aligned into natural wind coordinates (i.e. mean $w = 0$) (Kaimal and Finnigan, 1994); (3) offset for sensor lag (i.e. scan delay) between CSAT3 and LI-7500; (4) block averaged into 30-min periods to enable computation of instantaneous turbulence fluctuations; (5) corrected for frequency response (high/low-pass, and for physical sensor separation) and (6) applied density fluctuations specifically for gaseous fluxes (i.e. Webb *et al.*, 1980). Data observed instantaneously during storm events were omitted, as were measurements originating due east from the site (i.e. from wind direction 0–180°) to preclude turbulent flux measurements over non-representative LULC sectors, as well as wake turbulence generated from the tower's profile.

Selected tower data, such as Q^*, T_a and RH, were used to categorize distinct seasonal periods observed at WPHX. These data were complemented by ancillary hourly meteorological data corresponding with the measurement periods from the National Weather Service (NWS) station located at Phoenix Sky Harbor Airport. These were useful for stratifying seasonal flux tower data into clear-sky (i.e. no reported hourly cloud ceiling) *versus* non-clear, all-sky periods (excluding *in situ* measured precipitation events). Further, precipitation measured at
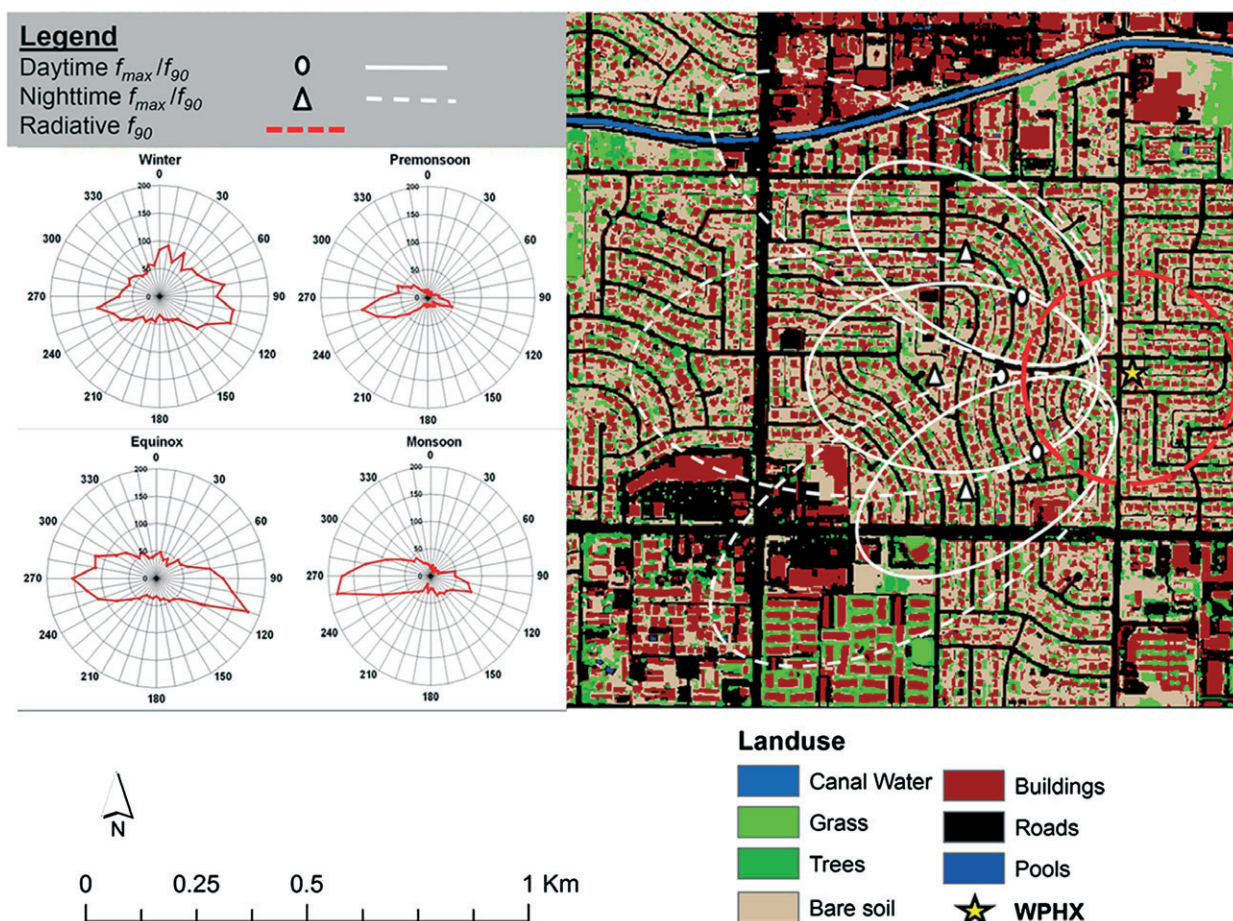
Figure 2. Seasonal wind roses based on wind data from WPHX (left), and LULC characteristics (with estimated footprints of both radiative and turbulent source areas) adjacent to tower site (right). Land cover classification object-based classification method employed by Myint *et al.* (2011) based on a 2011 Quickbird image of the WPHX neighbourhood with 2.4 m spatial resolution. Turbulent source area footprints were estimated with Schmid's (1994) FSAM for mean annual daytime and nighttime data for three wind directions – SW (180–240°), W (240–300°) and NW (300–360°). Note the preponderance of W winds at the tower site, as well as the large proportion of turbulent and radiative source areas originating over residential LULC at WPHX.

Sky Harbor was also used to quantify rainfall at WPHX due to the lack of an *in situ* rain gauge prior to February 2012. With these data, we classified four distinct seasons: winter, equinox, pre-monsoon and monsoon (Table 3). Note that both the vernal (March–May) and autumnal (September–November) equinox periods are analysed as a single season in this study. Periods with data loss due to equipment failure or instrument recalibration as well as the number of days with complete daily SEB data for analysis are also indicated in Table 3.

Generally, mean daily winter T_a was $<20\,^{\circ}$C, with mean $K_{inc} < 400\,\mathrm{W\,m}^{-2}$. Equinox periods are characterized by almost equal lengths of day and night, with mean daily T_a between 20 and $30\,^{\circ}$C. Summer conditions, with typically high mean K_{inc} and L_{inc} ($>500\,\mathrm{W\,m}^{-2}$ for both) and high daily $T_a > 30\,^{\circ}$C, were divided into distinct pre-monsoon and monsoon seasons. Although the NWS has, since 2008, redefined the summer monsoon period to June 15–September 30 for public safety reasons (Guido, 2009), we use the prior definition of three consecutive days with dew point temperatures above $12.8\,^{\circ}$C for meteorological analysis. On the basis of this, the start date of

the monsoon for the study period was on June 29, 2012. Lastly, to enable accurate comparisons with SEB data from other cities, as well as to correct for seasonal variations in solar time, all data are reported in Local Apparent Time (LAT) unless specified. On average, LAT is $\sim$0.5 h behind Local Time (LT) for WPHX.

We subsequently estimated the source area (or footprint) of the tower instruments (Figure 2), which were dependent on the type of flux measured. Estimation of the radiative flux footprint was relatively uncomplicated and could be ascertained as a circular source area centered on the radiometer based on its field-of-view and measurement height (Schmid *et al.*, 1991). The source area for turbulent fluxes, however, is dynamically dependent on several factors, such as wind direction and atmospheric stability (both of which are influenced by diurnal and seasonal patterns in weather), measurement height and surface roughness. On the basis of postprocessed micrometeorological data, we subsequently used Schmid's (1994) Flux Source Area Model (FSAM) to estimate mean annual footprints for turbulent fluxes within three upwind sectors at the tower; SW (180–240°), W

Table 2. Instrumentation installed at WPHX tower site.

Instrument/model	Manufacturer	Variable measured
Tower (all at 22.1 m AGL); 10 Hz sampling frequency; Installed November 2011		
3D sonic anemometer/CSAT3	Campbell Scientific	Three-dimensional wind velocities, virtual sonic temperature
Infrared gas analyzer/LI-7500	LI-COR Biosciences	Water vapour and carbon dioxide concentrations
Temperature–relative humidity sensor/HMP45AC	Vaisala	Air temperature and relative humidity
Net radiometer/NR01	Hukseflux	Incoming and outgoing short-wave and long-wave radiation
Near ground level (1.5 m AGL); installed February 2012		
Rain gauge/TB4	Hydrological Services	Total precipitation
BGL (between 0.02 and 0.3 m BGL); 1 Hz sampling frequency; installed March 2012		
Soil heat flux plate/HFP01SC	Hukseflux	Two sensors measuring bare soil and gravel ground heat fluxes corrected for 0.02 m BGL
Soil averaging thermocouple/TCAV	Campbell Scientific	Three sensors measuring soil temperatures at 0.05, 0.15 and 0.3 m BGL
Water Content Reflectometer/CS616	Campbell Scientific	Three sensors measuring soil volumetric water content at 0.05, 0.15 and 0.3 m BGL

AGL, above ground level; BGL, below ground level.

Table 3. Seasonal categories for data collected at WPHX in 2012, with start/end dates.

Season	Start/end dates (Year-Day number)	Sum total of days (days analysed with complete SEB data)[a]	Percentage of 30-min data occurring under clear-sky conditions	Mean sunrise (sunset) times (in LAT)
Winter	January 1–March 4 (YD 1–64) November 9–December 31 (YD 314–366)	117 (106)	78.35	0700 h (1700 h)
Equinox	March 5–May 9 (YD 65–129) September 11–November 8 (YD 255–313)	124 (81)	91.87	0600 h (1800 h)
Pre-monsoon	May 10–June 29 (YD 130–180)	51 (45)	99.97	0450 h (1900 h)
Monsoon	June 30–September 10 (YD 181–254)	74 (55)	77.53	0515 h (1900 h)

[a]Data loss due to laboratory re-zero and span of gas analyzer (winter, pre-monsoon) and from on-site power and sensor failure (equinox, monsoon).

(240–300°) and NW (300–360°), and derived the (1) mean distance of maximum upwind source weight (f_{max}) and (2) estimated source area isopleth at 90% (f_{90}) during both nighttime (stable) and daytime (unstable) conditions. We also compared the dimensions of the FSAM footprint, particularly f_{max}, with that derived from a simplified flux footprint model (Kljun *et al.*, 2002) that uses different variables from FSAM in estimating footprint size; in all cases, the difference between f_{max} in both models varied by <50 m for all sectors. In general, most measured turbulent flux densities originated from the appropriate LCZ 6 suburban LULC, especially during daytime where unstable conditions were prevalent, and in pre-monsoon and monsoon seasons where the majority of fetch was due west of the tower (Figure 2).

Given the implicit difficulties in estimating the heat storage in urban areas due to the complexity of the urban surface mosaic (Offerle *et al.*, 2005a; Roberts

et al., 2006), we assumed that the residual (RES) in the SEB Equation 1, i.e. $[Q^* - (Q_H + Q_E)]$, approximates that ΔQ_S as done in several other urban SEB studies (e.g. Coutts *et al.*, 2007; Newton *et al.*, 2007) and also represents the theoretical upper limit of ΔQ_S. Despite the observational and data postprocessing techniques utilized to reduce potential biases, this assumption accumulates all unavoidable measurement errors of other terms in Equation (1). Other urban EC campaigns (e.g. Christen and Vogt, 2004; Grimmond *et al.*, 2004; Moriwaki and Kanda, 2004) also note that turbulent fluxes are likely underobserved, especially at night when friction velocities (u_*) are low. These errors would influence energy balance closure, and our data interpretation will note this when necessary. Another potential complication when estimating ΔQ_S would be the influence of anthropogenic heat, i.e. Q_F within the study area, which has been shown to be a significant input to the SEB in several

cities (e.g. Sailor, 2011; Quah and Roth, 2012). Previous research by Grossman-Clarke *et al.* (2005), who used the inventory model proposed by Sailor and Lu (2004), estimated that (1) maximum hourly summer Q_F in metropolitan Phoenix across different LULC categories varied between ~20 and 35 W m^{-2}, with two distinct peaks corresponding with the morning and evening rush hours, and (2) mean daily (i.e. 24 h) summer Q_F at xeric residential LULC was ~25.5 W m^{-2}.

3. Results and discussion

3.1. Comparison of observed residuals with Q_G and modelled ΔQ_S

We utilized two approaches to examine the closure of Equation 1. First, ensemble mean hourly plots of directly measured ground heat flux density (Q_G) were obtained from two soil heat flux plates installed under distinct (1) bare sandy soil and (2) gravel mulch surfaces at the flux tower base. These sensors were installed after the winter season (Table 2), so comparative analyses of closure were only possible from March to December 2012. In the interpretation, we acknowledge the caveat of scale disparity between the Q_G measurements with the local-scale average from the tower residual, i.e. each heat flux plate measures an individual urban canopy facet *versus* an integrated signal from the complex, three-dimensional built environment. Second, we used the LUMPS model (V5.6) parameterized for the WPHX site (Table 4), which was concurrently run for the study's duration. LUMPS includes the Objective Hysteresis Model (OHM) that has been previously used to evaluate residual estimates from EC measurements in other suburban areas (Roberts *et al.*, 2006; Spronken-Smith *et al.*, 2006). Thus, ensemble

mean hourly all-sky data from the heat flux plates (Q_G), LUMPS (ΔQ_S) and the WPHX RES are illustrated together with the accompanying scatter plots from March to December 2012 (Figure 3).

The plots indicate that both consistent phase relationships (i.e. sign change between daytime *vs* nighttime) and trends are observed with both gravel and soil Q_G flux densities with respect to WPHX RES, although peak daytime and nighttime magnitudes of both Q_G fluxes are lower. Gravel surfaces are closer to RES, especially at night, possibly from its higher thermal admittance (μ) (Oke, 1987). By comparison, bare soil, which is more representative of the thermal properties of the neighbourhood's average LULC, shows greater disparities with the observed RES. Analysis of the diurnal energy balance closure using both heat flux plates (i.e. $Q^*-Q_G = Q_H + Q_E$) revealed a closure of ~63% (~83%) for sand (gravel) surfaces, with both having coefficients of determination of 0.88. These closure data are lower than reported in downtown Lodz (~95%) by Offerle *et al.* (2005a), but are within the range of reported closures across 22 FLUXNET sites (Wilson *et al.*, 2002).

By contrast, mean LUMPS ΔQ_S shows excellent fit with RES, with the lowest RMSE and highest r^2 and d (index of agreement) of three commonly used evaluation statistics (Willmott, 1982). This close relationship is especially evident at night ($\Delta Q_S < 0$), where a 1:1 ratio between observed RES *versus* modelled ΔQ_S is apparent. This good fit also appears from sunrise to noon, although ΔQ_S appears to systematically overestimate RES by ~50–75 W m^{-2} from 1200 to 1700 h, as well as lag RES by ~1 h. The latter feature was also observed in a similar comparison of diurnal tower residuals of a suburban site in Christchurch by Spronken-Smith *et al.* (2006). In general high agreement, as shown by the

Table 4. Selected LUMPS (Loridan *et al.*, 2011) and OHM parameters assigned for WPHX.

Model input parameters	Values assigned
Latitude/longitude	• 33.484083°/−112.143169°
Number of surface types in OHM	• 6
OHM inputs	• Canyons included with mean calculation of all coefficients
	• Calculation of vegetation coefficients is separated into grass/trees and shrubs/water using Asaeda and Ca (1993) and Doll *et al.* (1985)
	• Mean roof coefficients are utilized
	• Impervious areas are separated into concrete/asphalt and mean of all coefficients are used
Fractional cover of each surface type in .gis file[a]	• Buildings = 0.264
	• Paved = 0.22
	• Unmanaged soil = 0.368
	• Deciduous tree = 0.046
	• Grass = 0.101
	• Water = 0.01
Meteorological data inputs	• Hourly net radiation, downward long-wave radiation, mean wind speed, RH, T_a, wind direction, air pressure and hourly precipitation total from WPHX tower
	• Hourly observed cloud fraction from NWS Sky Harbor data
	• No anthropogenic heat flux input

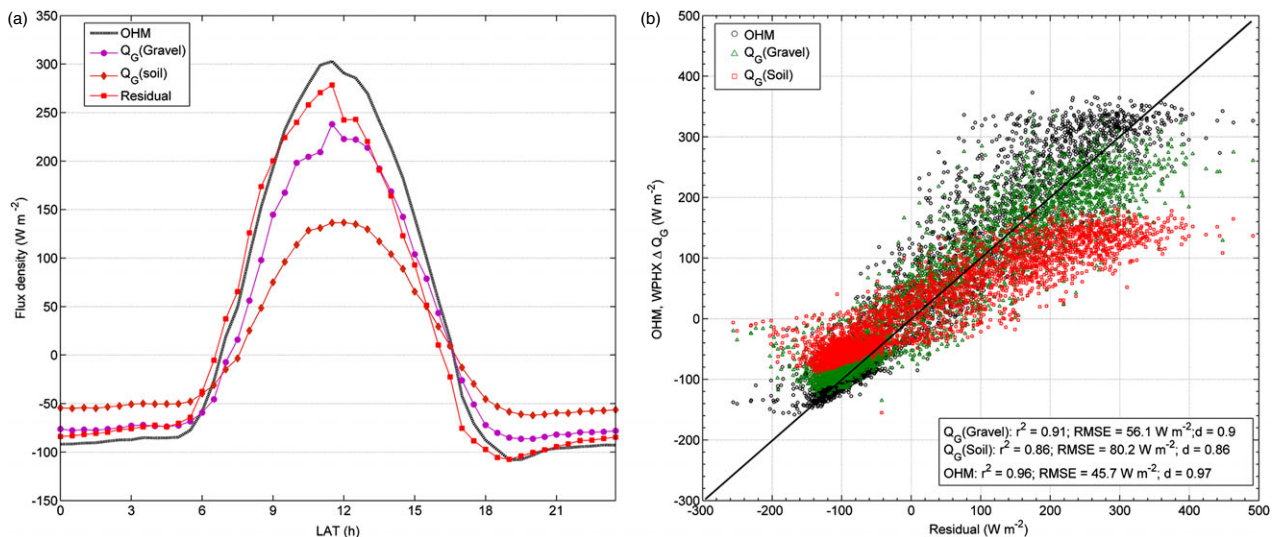[a]Based on Quickbird plan area land cover analysis in Table 1.

Figure 3. Ensemble mean hourly all-sky data from WPHX heat flux plates (Q_G) under gravel and soil surfaces from LUMPS (OHM) and the WPHX residual from March to December 2012 (a), and scatter plots of Q_G and OHM *versus* the residual RES (b). Solid diagonal line in scatter plots indicates 1:1 ratio. r^2, coefficient of determination; RMSE, root mean square error; d, index of agreement (Willmott, 1982). The relatively close agreement in trend and magnitude of RES with the LUMPS ΔQ_S, especially at night, suggests that the tower residuals are a reasonable estimate of the 'actual' urban ΔQ_S.

overall high d for both heat flux plates and LUMPS, suggests that the residual from the tower is a reasonable estimate of the ensemble ΔQ_S term, at least during the March to December 2012 period.

3.2. Meteorological and radiation conditions – seasonal variations in meteorology and energy fluxes

We examined the annual pattern of the directly measured SEB fluxes, together with selected meteorological variables that were observed at WPHX (Figure 4). Mean all-sky daily (24 h) time-series plots of (1) incoming and outgoing long- and short-wave radiation, (2) ambient air temperature, wind and humidity conditions, (3) SEB fluxes and (4) soil moisture and site precipitation at WPHX during 2012 were used to illustrate distinct seasonal variations in the dataset (Figure 4). Note that data shown in (a–c) were plotted as 5-day moving averages to minimize diurnal variability of synoptic weather patterns, but 1-day averages of soil moisture and total precipitation are illustrated in (d).

Peak magnitudes of mean K_{inc} are observed during the pre-monsoon period, which are characterized by cloud-free conditions due to persistent anticyclonic conditions aloft (Figure 4(a)). A notable decrease in K_{inc} occurs during the start of the monsoon period, which also corresponds with peak magnitudes of L_{inc} and L_{out} arising from greater surface and atmospheric moisture conditions (e.g. greater soil moisture and cloud cover). Seasonal trends of K_{out} were similar to K_{inc}, which also translated to largely consistent albedo ($\alpha = K_{out}/K_{inc}$) measured throughout the year. Mean noon α measured under all-sky conditions was relatively consistent in all seasons – 0.172 in the pre-monsoon, 0.169 during the equinox, 0.168 during the winter and 0.166 during the monsoon, with a small

decrease possibly due to increased surface soil moisture and vegetation greening resulting from greater precipitation. The measured WPHX α is notably similar in magnitude to data observed in other suburban residential areas (~0.15) (Oke, 1988; Offerle *et al.*, 2006).

Indicative of the hot arid climate in Phoenix are the high mean T_a and large mean vapour pressure deficit (VPD) that are usually experienced during the summer months both pre-monsoon and monsoon seasons (Figure 4(b)). A large VPD typical of the desert climate also persists, despite the significantly greater precipitation observed during the monsoon *versus* pre-monsoon. Slightly larger wind speeds (both mean daily u and u_*) are observed during the summer months, which contrast with the generally less turbulent conditions during non-storm periods in winter. Lastly, a diurnal east-to-west switch in average wind direction recorded at the site is notable in the large quantity of E–W winds sampled *in situ* (Figure 2), which results from a regular evening transition of anabatic and katabatic flows that has been well documented in metropolitan Phoenix (Brazel *et al.*, 2005).

Seasonal variations in $Q*$ appear to control corresponding variations of the turbulent fluxes Q_H and Q_E (Figure 4(c)). Mean daily $Q_H > Q_E$ throughout the year, which is similar to SEB data from most other urban sites (e.g. Offerle *et al.*, 2006). Larger absolute flux densities were seen during the summer months; however, a clear difference in timing exists between mean peak Q_H (pre-monsoon; ~100 W m^{-2}) and Q_E (monsoon; ~70 W m^{-2}). While generally turbulent pre-monsoon conditions could account for the large average Q_H, the longer day lengths and higher sun angle, coupled with largely dry and cloud-free conditions close to the solstice at WPHX, could also explain this seasonal peak in Q_H.
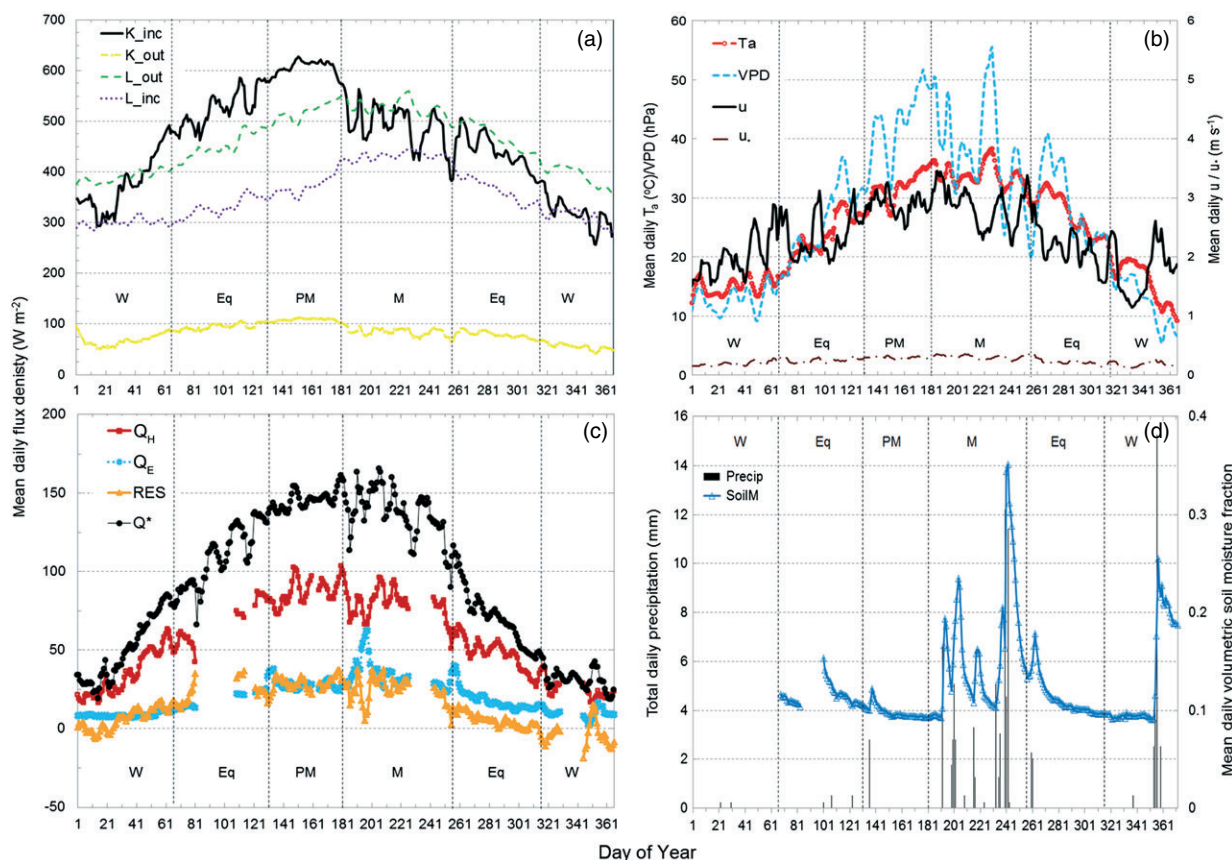
Figure 4. Seasonal variations of weather and SEB fluxes are displayed as 5-day, all-sky moving averages of selected mean daily (24 h) variables at WPHX. These include (a) incoming (inc) and outgoing (out) short-wave (K) and long-wave (L) radiation; (b) air temperature (T_a), vapour pressure deficit (VPD), wind speed (u) and friction velocity (u_*); (c) sensible heat (Q_H), latent heat (Q_E), residual (RES) and net all-wave radiation (Q^*), and (d) total daily precipitation (Precip) and mean (one-day averaged) soil moisture fraction at 0.05, 0.15 and 0.3 m depths (SoilM). Seasonal periods are indicated by the following acronyms: W, Winter; Eq, Equinoxes; PM, Pre-monsoon; and M, Monsoon. NB: gaps in SEB data in (c) are due to instrument calibration or failure, and reported precipitation data in (d) prior to YD 31 are from Sky Harbor Airport meteorological station.

The increased pre-monsoonal solar impact results in greater irradiation of urban surfaces (i.e. less shadows within urban canyons) translating to equilibrium temperatures being reached earlier in the day. In contrast, peak seasonal Q_E corresponds with monsoonal rainfall events (Figure 4(d)). A prominent series of monsoon storms from YD 192–205 resulted in a distinct spike in mean daily Q_E – coupled with corresponding decreases in both Q_H and RES – that persisted for several days. This was probably due to evaporation of increased soil moisture from porous surfaces within WPHX during post-storm drying periods. It was unfortunate that sensor failure during the late monsoon (YD 231–245) prevented direct measurement of Q_E when soil moisture appeared to be at or near field capacity due to accumulated antecedent precipitation from a series of storms; it is probable that measured mean daily Q_E would have been at a maximum during this period.

Assuming both instrumentation errors and ΔQ_A to be relatively minor due to careful site selection, frequent sensor maintenance and data filtering/postprocessing, the RES term should equate to the sum of ΔQ_S and Q_F fluxes measured at WPHX. Over longer time periods (e.g.

1-day or over multiple days), ΔQ_S should approximate to zero as unrealistic heating or cooling of the urban surface would entail otherwise (e.g. Pigeon *et al.*, 2007). While the 5-day averaged daily RES is close to zero (and even negative) during winter and the autumnal equinox, the net positive RES observed at WPHX strongly suggests that Q_F is a significant contributor at WPHX over the course of the year. This is true especially during the vernal equinox and summer months where mean daily RES is consistently ∼25 W m^{-2}, which is of a similar magnitude to estimated residential Q_F calculated in Grossman-Clarke *et al.* (2005). This is likely due to waste heat inputs from the constant operation of residential air conditioning within the study area. The influence of Q_F is not restricted to space cooling, as a notable frontal winter storm (YD 353) corresponded with a short spike in RES, probably from residential heating as a reaction to the sudden reduced T_a.

3.3. Diurnal and seasonal ensemble SEB profiles

We plotted the ensemble means of diurnal 30-min SEB flux profiles for each season under both all-sky and clear-sky conditions (Figure 5). We included these plots for
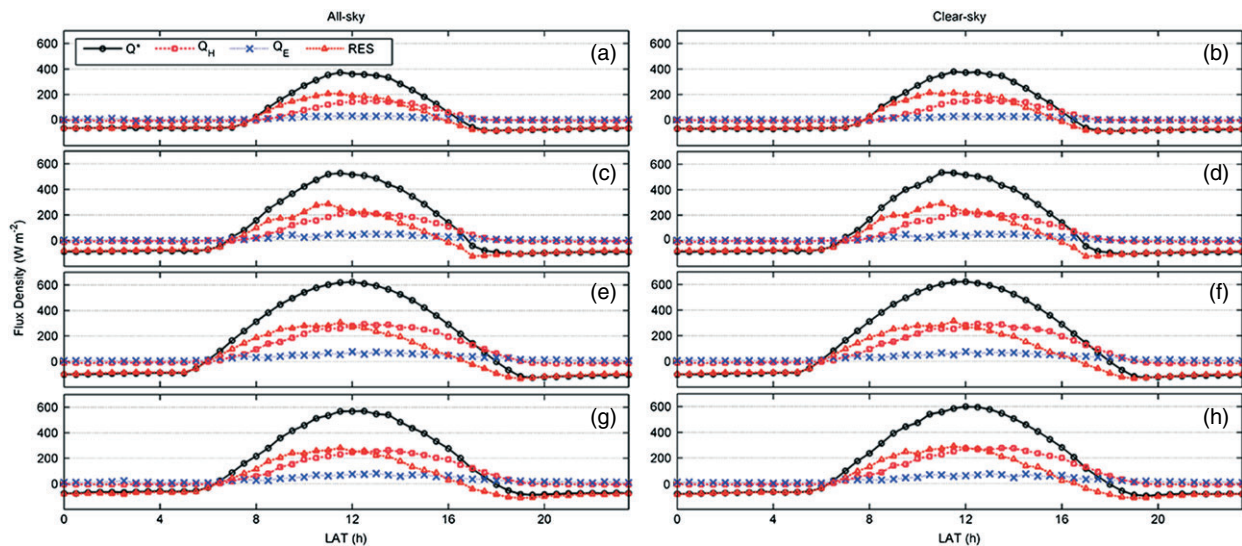
Figure 5. Ensemble means of 30-min averaged SEB fluxes (in $W\,m^{-2}$) under winter (a, b), equinox (c, d), pre-monsoon (e, f) and monsoon (g, h) seasons during all-sky (left column) and clear-sky (right column) conditions. Note the lack of significant variation in ensemble means between weather categories. The sign convention is that turbulent energy terms (i.e. Q_H and Q_E) are positive in magnitude when directed away from the surface, and negative when directed towards the surface for the terms $Q*$ and RES.
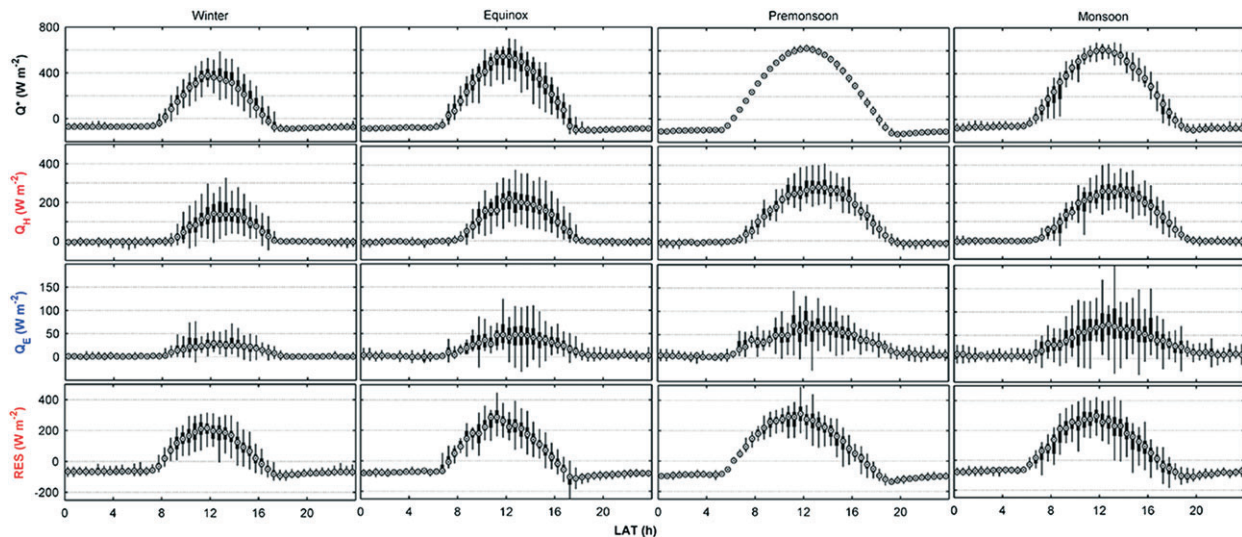

Figure 6. Box plots of ensemble mean seasonal SEB fluxes observed under all-sky conditions. Medians are the circled dots; the bottom (top) of each box represents the first (third) quartile, and the bottom (top) whiskers represent minima and maxima values, respectively. Sign convention is similar to Figure 5. A notable change in data spread – especially with Q_E – is observed during the wet monsoon season.

all-sky conditions as there were insufficient postprocessed non-clear sky data (i.e. rain or cloud influences) to plot complete ensemble daily means for all seasons (Table 3). Diurnal and seasonal variability of each SEB component were also illustrated through box plots of data measured under all-sky conditions (Figure 6). Apart from a small reduction in mean all-sky peak $Q*$ during the solar noon of the monsoon season (possibly from cloud cover impacts), there was an overall lack of significant variation between all-sky and clear-sky ensemble mean SEB for all seasons, especially during the pre-monsoon; however, the influence of weather can be discerned during other seasons in which larger SEB flux data variability is apparent in the box plots. Peak daytime $Q*$ in all seasons occurred

between 1200 and 1230 h, with greater flux magnitudes during the summer months *versus* winter (600 and 390 $W\,m^{-2}$, respectively). The largest nocturnal $Q*$ flux consistently occurred just after sunset during all seasons.

Largest daytime SEB flux densities are generally partitioned into RES, followed by Q_H and Q_E terms, respectively. The timing of each flux maxima also varies; in all seasons, RES peaks just before solar noon, while maxima of Q_H and Q_E occur in the afternoon. All fluxes displayed greater variability during the daytime for every season (Figure 6). Of interest is the average daytime timing of the critical flux phase when turbulent energy dominates, i.e. $Q_H > $ RES, which occurs significantly earlier in pre-monsoon (1200 h) relative to winter (1400 h), likely

from a combination of greater wind speeds, higher solar angle and longer day lengths. During all seasons, nocturnal SEB fluxes are largely dominated by conduction and radiation from the RES term. There is also rapid (1–2 h) surface cooling immediately after sunset during all seasons which is manifest by sharp declining trend in RES, before levelling off by 1–2 h after sunset. The diurnal development of urban SEB fluxes at WPHX bears some similarity to other cities in arid/highland climates (i.e. B and H Köppen climates) with little vegetation cover. For instance, data from Tucson (Grimmond and Oke, 1995), suburban Mexico City (Oke *et al.*, 1992; Tejeda-Martinez and Jauregui, 2005), Mexicali (Garcia-Cueto *et al.*, 2003) and Ouagadougou (Offerle *et al.*, 2005b) all show periods when RES (or the ΔQ_S term) $> Q_H$ after sunrise, before the latter dominates surface energy exchanges at some point after solar noon. The timing of this switch appears to be directly related to surface evapotranspiration, with drier cities with lower observed peak Q_E (i.e. Mexico City, Mexicali and Ouagadougou) all having a later phase change. Interestingly, this post-noon transition is also observed in the mid-latitude city of Tokyo during the dry winter season, where peak Q_E is substantially less than in summer (Moriwaki and Kanda, 2004).

The ensemble mean RES shows similar diurnal trends in all seasons, with large negative (i.e. away from the surface) nocturnal flux densities that decrease in magnitude upon sunrise, with a change in sign occurring ~1 h thereafter as insolation is absorbed by the urban surface. Peak RES is consistently reached at ~1130 h, before gradual decreasing towards zero by 1530 h (winter and equinox) and 1600 h (summer). Thereafter, negative RES fluxes strengthen until levelling off at ~1700 h (winter and equinox) and 1900 h (summer), before slightly diminishing in magnitude and remaining stable thereafter throughout the night. Seasonally, largest average daytime clear-sky RES occurs in the pre-monsoon (315 W m^{-2}), followed by equinox (310 W m^{-2}), monsoon (291 W m^{-2}) and winter (213 W m^{-2}). The largest nighttime magnitudes follow the same seasonal classification [between −88 (winter) and 134 W m^{-2} (pre-monsoon)], which may be related to greater measured nocturnal cloud cover measured at Sky Harbor during the three other seasons that inhibits surface radiative cooling compared to the clear pre-monsoon period. The timing of peak daytime RES before solar noon is similar to other tropical and subtropical cities (Roth, 2007), but peak summer RES fluxes in WPHX exceed those recorded in other cities, with the highest peak daytime RES documented in downtown Mexico City (~275 W m^{-2}) (Oke *et al.*, 1999), although with the proviso that additional Q_F input from summertime residential air conditioning use may account for the large RES magnitude in WPHX. Nocturnal RES is, however, comparable in both magnitude and trend to those observed in Tucson in April (Grimmond and Oke, 1995), and in downtown Mexico City during the dry season (Oke *et al.* 1999).

At night, mean Q_H is small in magnitude (−5 to −10 W m^{-2}) but generally negative in flux (i.e. towards

the surface; ~71.1% of total Q_H observations) during all seasons. During the day, a change in sign of Q_H generally occurs ~1.5 h after sunrise, before increasing in magnitude until a peak between 1 and 2 h after solar noon. Largest mean hourly clear-sky Q_H occurs in the pre-monsoon (292 W m^{-2}), followed by monsoon (291 W m^{-2}), equinox (219 W m^{-2}) and winter seasons (151 W m^{-2}). Subsequently, Q_H decreases and changes sign ~0.5 h after sunset in all seasons, subsequently remaining negative until sunrise in general. This feature could be linked to the strong radiative cooling that facilitates regular nocturnal inversions, which suppresses turbulent convectional processes. The peak daytime summer Q_H is similar in flux to most mid-latitude (Grimmond and Oke, 2002) and tropical cities (Roth, 2007), though net negative Q_H after sunset at WPHX is not a universal feature. Oke *et al.* (1999) and Christen and Vogt (2004) noted positive nocturnal Q_H in downtown Mexico City and Basel, respectively, which is possibly due to a large H/W or aspect ratio that increases surface roughness and reduces surface long-wave cooling; however, persistent and slightly negative Q_H fluxes were also found in subtropical urban sites with typically low H/W ratios that were located in Miami (Newton *et al.*, 2007) and Cairo (Frey *et al.*, 2011).

Given the xeric land cover at WPHX, magnitudes of Q_E are significantly less compared to RES and Q_H. The diurnal development of Q_E differs from the other fluxes in that, on average, it is generally positive in sign throughout the 24-h period (~78.6% of total 24 h observations). Mean Q_E increases until the daytime maxima is reached just after solar noon, before decreasing and levelling off to a constant low flux after sunset. Minute Q_E fluxes are generally directed away from the surface (2–5 W m^{-2}) throughout the night in all seasons (~75.7% of total nocturnal observations). The largest mean hourly clear-sky Q_E fluxes were found during the monsoon (76 W m^{-2}), followed by pre-monsoon (74 W m^{-2}), equinox (53 W m^{-2}) and winter (29 W m^{-2}). A small but noticeable peak in median Q_E (<15 W m^{-2}) is also present just after sunrise during the equinox and summer months (Figure 6), which could suggest the influence of *ad-hoc* irrigation of vegetation within WPHX. Evaporation of localized dewfall could also be a possibility, although the large daily VPD year-round may preclude this.

Seasonal analysis of all-sky *versus* clear-sky Q_E shows that the influence of the monsoon is apparent with more energy partitioned into Q_E at the expense of RES, which is expected in (sub)tropical cities subject to frequent precipitation (Roth, 2007). Although larger peak Q_E fluxes, especially during daytime, are documented in the monsoon *versus* pre-monsoon, there appears to be no significant difference in magnitude between mean (Figure 5) or median (Figure 6) pre-monsoon and monsoon Q_E fluxes, despite the larger and more frequent observed monsoonal precipitation (Figure 4(d)). When compared to fluxes at sites in other subtropical cities, mean daytime summer Q_E in WPHX is lower

than those at Tucson, Miami and a suburban Mexico City site. Daytime summer Q_E is also similar to fluxes measured at Ouagadougou, but it is greater than those observed at Mexicali (Garcia-Cueto *et al.*, 2003), downtown Mexico City and Cairo. Nocturnal mean Q_E fluxes in all seasons, however, are among the lowest documented in the urban SEB literature, comparable to the very dry sites of Mexicali, downtown Mexico City, and Cairo.

3.4. Temporal trends in normalized and total energy partitioning

To aid with examining relative SEB partitioning trends and to also facilitate direct comparison with other clear-sky SEB data reported in other cities, we plotted mean ratios of each flux normalized by net all-wave radiation under clear-sky conditions (i.e. $\chi = Q_H/Q^*$, $\gamma = Q_E/Q^*$, $\Lambda = RES/Q^*$, $\beta = Q_H/Q_E$) (Figure 7). Large magnitudes of each flux ratio occur close to sunrise or sunset, but these results from division by very small numbers are thus not significant.

The diurnal and seasonal analysis of normalized SEB reveals distinctive hysteresis patterns of χ and Λ that clearly mirror each other, which has been observed in other cities (e.g. Grimmond and Oke, 1995; Roth, 2007). During daytime in all seasons, mostly positive magnitudes of χ increase from zero from sunrise until it contributes ~70% of net flux ~1 h before sunset (Figure 7(a)). In contrast, almost all of net SEB fluxes are partitioned into Λ at sunrise (Figure 7(c)); gradually decreasing to ~25% at the same time that peak χ occurs. This pattern is indicative of increasing daytime near-surface instability at WPHX resulting in greater transfer of surface energy through convection as opposed to conduction and/or radiation. Nighttime trends of χ and Λ both stabilize after a sharp drop immediately after sunset towards zero and one, respectively.

The consistent diurnal hysteresis seen in both χ and Λ during all seasons is similar to other cities in all climate zones (Grimmond and Oke, 2002; Newton *et al.*, 2007; Roth, 2007), with a constant increase (decrease) in χ (Λ) from sunrise until sunset. The progression of these mirroring trends corresponds to a boundary-layer daytime development from static stability to instability, where surface energy loss favours convection over conduction, especially in the late afternoon. Conversely, the regularly low (high) nocturnal χ (Λ) implies a stable or neutral boundary layer in all seasons, which has implications towards low-level mixing and air quality at WPHX. This consistent trend regardless of season suggests that the parameterization of these normalized terms of χ and Λ for the purpose of urban climate modelling in the WPHX context is likely robust, with the proviso that these normalized terms are derived under clear-sky weather conditions.

γ, however, generally contributes <15% of net flux during the day, with substantially lower magnitudes during winter (~8%) *versus* other seasons months (equinox and pre-monsoon = ~12%; monsoon = ~15%) (Figure 7(b)). A regular switch in sign in the day (positive) and night (negative) occurs due to ensemble mean diurnal Q_E generally being positive in sign. Notably, trends and magnitudes of pre-monsoon and monsoon γ are similar, despite the larger precipitation and soil moisture observed during the latter. This non-difference could, however, arise from analysing only clear-sky (and not all-sky) SEB data, as Q_E does have a strong influence on energy transfer immediately after monsoonal or winter storms can persist for several days (Figure 4). The consistently low magnitudes and diurnal trends of mean clear-sky γ are unsurprising, and mean summer WPHX γ are lower *versus* those derived in Tucson, but mean winter γ is similar to other observed dry sites in Mexicali (Garcia-Cueto *et al.*, 2003) and downtown Mexico City (Oke *et al.*, 1999); although these latter two locations
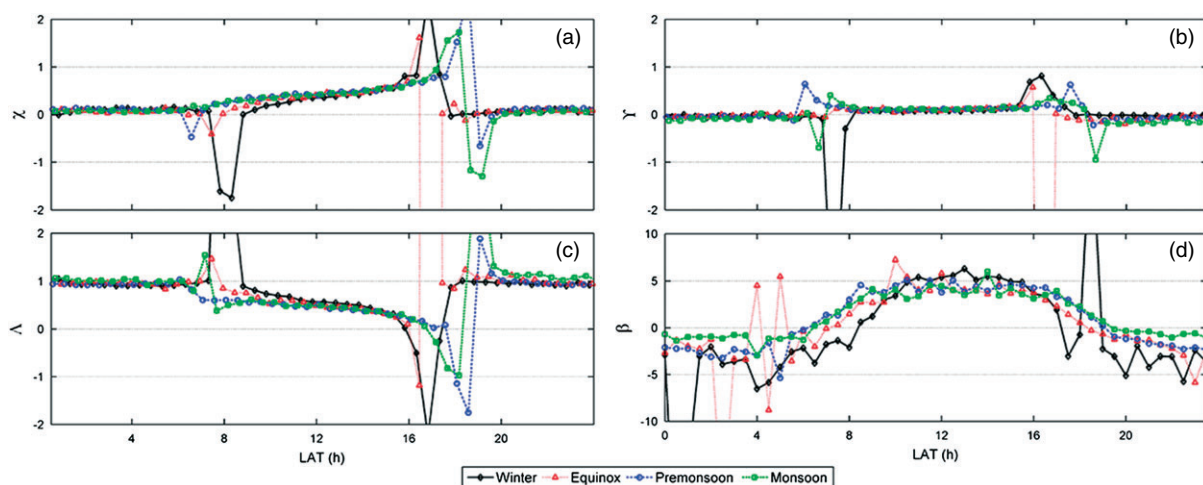

Figure 7. Clear-sky ensemble diurnal means of (a) χ (Q_H/Q^*), (b) γ (Q_E/Q^*), (c) Λ (RES/Q^*) and (d) β (Q_H/Q_E). Note the consistent hysteresis between plots (a) and (c), as well as the increase in flux partitioning towards Q_H during daytime hours. Large magnitudes close to sunset and sunrise are due to division by small numbers, and can be ignored.
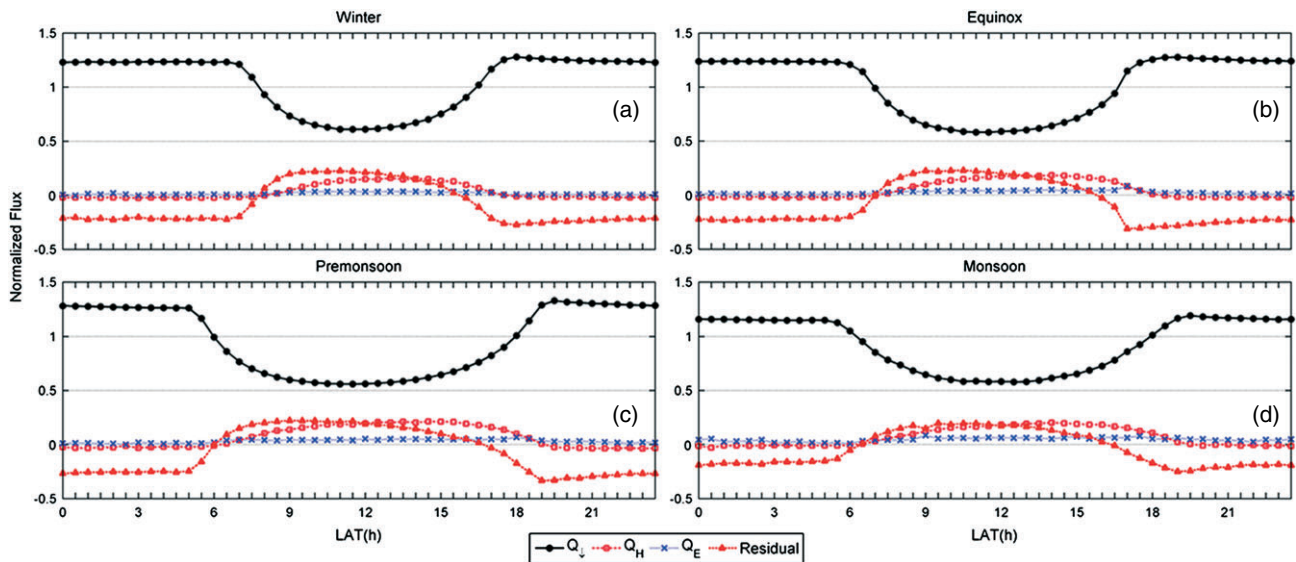
Figure 8. Mean ensemble diurnal flux ratios normalized by total incoming radiation ($Q_\downarrow$) at WPHX during winter (a), equinox (b), pre-monsoon (c) and monsoon (d) seasons under clear-sky conditions. Positive normalized magnitudes of $Q_\uparrow$, Q_H and Q_E indicated energy lost from the surface and vice versa. The opposite holds for RES.

have much less reported proportional vegetation cover compared to WPHX.

The temporal analysis of the Bowen ratio of observed turbulent fluxes (β) indicates the relative importance of Q_H throughout the year, especially during the $\pm 3\,h$ period around solar noon where $\beta = 4$ for all seasons (Figure 7(d)). Small inter-seasonal differences exist, with winter and equinox $\beta >$ summer β, and daytime monsoonal β unsurprisingly being slightly lower *versus* the drier pre-monsoon period. At night, due to the prevailing negative Q_H fluxes, mean β is generally negative during all seasons. This feature, where Q_H is generally negative but Q_E is positive in flux, probably arises from the combination of a nocturnal radiative inversion that inhibits convection, coupled with consistent dry air advection over patchy irrigated surfaces within the study area that facilitates and supplements energy released by RES in vapourizing surface moisture (Oke, 1988). When compared to other cities, mean daytime β derived at WPHX is at the upper limit of the range of urban β (Grimmond and Oke, 2002; Roth, 2007), and much higher than in mid-latitude cities (Grimmond and Oke, 1995; Spronken-Smith, 2002; Moriwaki and Kanda, 2004) and in several Köppen *B* climate cities (Newton *et al.*, 2007; Roth, 2007; Frey *et al.*, 2011). However, mean daytime β is less than measured at Mexicali, Vancouver (Grimmond and Oke, 1999) and in downtown Mexico City. Nocturnal trends of mostly negative β are similar to most other sites, regardless of climate classification.

A recent criticism of normalization of SEB fluxes over $Q*$ is that it includes surface characteristics (e.g. albedo and emissivity) that may vary between and within urban sites, and normalizing the SEB instead via total incoming radiation ($Q_\downarrow$) would facilitate comparisons that are independent of the underlying urban surface (Loridan and Grimmond, 2012). We have thus included

plots of clear-sky, ensemble seasonal mean diurnal SEB flux ratios normalized by $Q_\downarrow$ (Figure 8). Temporal trends utilizing this method are similar to trends in SEB fluxes in Figure 5 in terms of (1) relative daytime *versus* nighttime magnitudes of each flux, (2) timing of phase change between the importance of Q_H *versus* RES and (3) the seasonal differences in SEB fluxes. Of interest is the comparison of these average normalized fluxes with other cities, especially with respect to flux ratios observed during mean midday (i.e. $\pm 3\,h$ around solar noon) period indicative of the peak efficiency of surface-atmosphere energy transfer (Loridan and Grimmond, 2012, Table 2). Winter is the only season where the normalized ratio of daytime turbulent fluxes are less than the residual (RES $= 0.186 Q_\downarrow$; $Q_H + Q_E = 0.158 Q_\downarrow$), a characteristic similar to those observed at the downtown Mexico City tower, and at the suburban Melbourne site in winter (Coutts *et al.*, 2007). The increasing influence of turbulent fluxes in energy transfer with greater day length and solar angle during the equinox (RES $= 0.182 Q_\downarrow$; $Q_H + Q_E = 0.199 Q_\downarrow$), pre-monsoon (RES $= 0.182 Q_\downarrow$; $Q_H + Q_E = 0.234 Q_\downarrow$) and monsoon seasons (RES $= 0.161 Q_\downarrow$; $Q_H + Q_E \sim 0.236 Q_\downarrow$) is similar in trend to long-term sites in Melbourne, Helsinki (Vesala *et al.*, 2008) and Lodz (Offerle *et al.*, 2006). With respect to short-term sites, magnitudes of $Q_H + Q_E$ measured at WPHX fall between data reported from an industrial Vancouver site with little surface vegetation (Grimmond and Oke, 1999) and a subtropical coastal site in Miami (Newton *et al.*, 2007).

We also summarized mean total 24 h radiant and turbulent energy received at WPHX according to clear-sky *versus* all-sky conditions for all SEB fluxes and its normalized ratios; these data were tabulated for each month and season (Table 5). The development of each mean daily SEB flux with respect to variations in $Q*$

Table 5. Summary of mean daily total SEB fluxes (MJ m^{-2} day^{-1}) and derived unit-less flux ratios for each month and season categorized under clear-sky and all-sky conditions.

Month (total days sampled)/**Season**	$Q*$	Q_H	Q_E	RES	χ	γ	Λ	β
Clear-sky conditions only – daily (24 h)								
January ($n = 15$ days)	2.79	1.80	0.69	0.30	0.65	0.25	0.10	2.62
February ($n = 19$)	5.98	3.92	0.76	1.29	0.65	0.13	0.22	5.14
March ($n = 11$)	7.12	4.96	1.06	1.10	0.70	0.15	0.15	4.68
April ($n = 4$)	9.18	5.69	1.47	2.02	0.62	0.16	0.22	3.87
May ($n = 18$)	12.39	7.44	2.28	2.67	0.60	0.18	0.22	3.26
June ($n = 24$)	12.78	7.73	2.39	2.65	0.61	0.19	0.20	3.23
July ($n = 20$)	13.11	7.34	2.80	2.97	0.56	0.21	0.23	2.62
August ($n = 6$)	12.36	7.27	2.36	2.73	0.59	0.19	0.22	3.08
September ($n = 26$)	8.93	5.66	1.93	1.35	0.63	0.22	0.15	2.93
October ($n = 26$)	5.35	3.74	1.25	0.35	0.70	0.23	0.07	2.99
November ($n = 10$)	3.57	2.49	1.00	0.09	0.70	0.28	0.02	2.49
December ($n = 14$)	2.18	1.81	0.73	−0.36	0.83	0.33	−0.16	2.48
Winter total	**3.99**	**2.80**	**0.79**	**0.40**	**0.70**	**0.20**	**0.10**	**3.54**
Equinox total	**7.03**	**4.61**	**1.44**	**0.98**	**0.66**	**0.20**	**0.14**	**3.20**
Pre-monsoon total	**12.65**	**7.61**	**2.38**	**2.66**	**0.60**	**0.19**	**0.21**	**3.19**
Monsoon total	**12.41**	**7.24**	**2.50**	**2.67**	**0.58**	**0.20**	**0.21**	**2.90**
All-sky seasonal conditions – daily (24 h)								
January ($n = 31$)	2.77	1.96	0.71	0.10	0.71	0.26	0.03	2.76
February ($n = 29$)	5.67	3.90	0.78	1.00	0.69	0.14	0.18	5.02
March ($n = 17$)	7.26	4.80	1.13	1.33	0.66	0.16	0.18	4.25
April ($n = 4$)	10.20	6.22	1.63	2.34	0.61	0.16	0.23	3.82
May ($n = 30$)	12.16	7.31	2.45	2.40	0.60	0.20	0.20	2.99
June ($n = 24$)	12.84	7.79	2.43	2.61	0.61	0.19	0.20	3.21
July ($n = 31$)	12.55	6.92	3.33	2.30	0.55	0.27	0.18	2.07
August ($n = 11$)	12.25	7.22	2.63	2.40	0.59	0.21	0.20	2.74
September ($n = 30$)	8.44	5.20	2.21	1.03	0.62	0.26	0.12	2.35
October ($n = 31$)	5.59	4.03	1.30	0.27	0.72	0.23	0.05	3.11
November ($n = 18$)	3.77	2.78	1.07	−0.09	0.74	0.29	−0.02	2.59
December ($n = 31$)	2.60	1.91	0.82	−0.14	0.74	0.32	−0.05	2.32
Winter total	**3.64**	**2.61**	**0.80**	**0.23**	**0.72**	**0.22**	**0.06**	**3.26**
Equinox total	**7.01**	**4.58**	**1.61**	**0.82**	**0.65**	**0.23**	**0.12**	**2.84**
Pre-monsoon total	**12.61**	**7.56**	**2.49**	**2.56**	**0.60**	**0.20**	**0.20**	**3.04**
Monsoon total	**12.01**	**6.84**	**2.99**	**2.18**	**0.57**	**0.25**	**0.18**	**2.29**
Annual total (GJ m^{-2} year^{-1})	**3.40**	**2.13**	**0.76**	**0.51**	**–**	**–**	**–**	**–**

over the course of the year is clear, with largest flux densities in the summer months of June and July. Of note is the large relative influence of Q_H (and a high β) at the end of the winter season in February, which subsequently decreases in relative importance with respect to Q_E. This trend is reflected in the decrease of June and July χ (and a corresponding increase in γ) under both clear-sky and all-sky conditions. While trends of Λ are close to zero in the winter months, mean clear-sky daily Λ appears to be consistently negative in December, which is a feature also seen in several cold climate cities e.g. Lodz (Offerle *et al.*, 2006). When contrasted with other North American cities with comparable daily summertime SEB datasets, i.e. Tucson, Chicago and Sacramento (Grimmond and Oke, 1995), pre-monsoonal data at WPHX have the largest magnitudes of total daily $Q*$ and Q_H. Part of this result could stem from WPHX's geographical location, but this may also arise from the more complete dataset from here compared to the much smaller periods sampled in the earlier studies. Lastly, as noted above, the relatively high 24 h summer Λ – especially with respect to γ – suggests that Q_F inputs at WPHX through waste

residential heat during the pre-monsoon and monsoon months should be considered as an important factor in its SEB, possibly contributing ~20% of mean daily fluxes within the neighbourhood.

3.5. Relation of urban surface characteristics at WPHX with observed fluxes

We can infer several features about the local surface characteristics given the consistent and overall high degree of partitioning into the RES and Q_H terms due to the relatively low evapotranspiration at WPHX. The large proportion of radiation forcing stored into the ensemble subdaily RES term during all seasons is indicative of the high μ relative to the desert surroundings. Two factors can explain the high μ at WPHX; the large quantity of urban fabric at the site and the three-dimensional urban mosaic of combined active surfaces (e.g. walls, roofs and roads) that enhances and increases net radiation absorption in cities, especially during winter where solar angles and daylight hours are less, and the vertical building walls being more efficient in absorbing solar irradiance. However, the dynamics of SEB fluxes are also influenced

by the urban cover and structure at WPHX, which can be inferred from the predominant negative nocturnal Q_H. Despite the large nocturnal RES, the suburban structure of this area, evident by the low mean H/W and high mean Ψ_S, lacks a dense urban geometry to sustain an upward sensible heat flux after sunset (e.g. Oke, 1988), as it would in a downtown urban core or at a site with a greater proportion of impervious surfaces, e.g. Mexico City (Oke *et al.*, 1999). The relatively earlier timing of the switch from positive to negative Q_H compared to other subtropical suburban sites in Miami and Cairo also suggests the role of low-density (i.e. low mean aspect ratio or H/W) urban structure as an important control of urban Q_H.

With the low proportion of likely evapotranspiration sources within WPHX, the reported magnitudes of ensemble daytime Q_E flux during the dry pre-monsoon (Figure 6), coupled with its large daytime variability, are a notable result especially when ensemble mean diurnal and total daily Q_E are similar in magnitude to the monsoon season (Figure 5; Table 5). Examination of the urban structure shows that pervious surfaces (i.e. bare soils and vegetation) contribute about half of the plan area land cover (Figure 2; Table 1), suggesting the possibility of a large evaporative moisture supply from these pervious surfaces to the urban atmosphere based upon the likelihood that water on impervious surfaces in WPHX are either rapidly run-off or ephemerally stored for only a few hours. The presumptive water source from porous soils and vegetation is, however, misleading given the perennially low soil moisture present within xeric residential areas in Phoenix (e.g. Zhu *et al.*, 2006; Gober *et al.*, 2010), which is supported by measurements at the base of the WPHX tower during non-storm periods (Figure 4(d)). Further, potentially pervious or porous urban fabric in WPHX that could be an evaporation source after storm events is instead likely to have strongly diminished porosity due to the persistently dusty environment. Soil pores are especially prone to clogging during the frequent summer dust storms that occur in Phoenix. During the dry pre-monsoon, with little precipitation combined with minimal irrigation of non-vegetated surfaces, it is probable that evaporation from bare soil and gravel surfaces is negligible during this season. This feature implies that the only readily available moisture source at that period would originate from vegetated surfaces and pools, when filled.

Assuming no other anthropogenic moisture inputs (e.g. evaporative cooling towers), we can roughly estimate the mean peak hourly latent heat flux per unit natural coverage as applied by Moriwaki and Kanda (2004) for Tokyo [i.e. $Q_{E(natural)} = Q_E/$(cumulative fraction of pools, grass and trees)]. While this method neither accounts for the nature of three-dimensional urban surface, which may be problematic in urban environments with low Ψ_S [e.g. LCZ 1 or 4 from Stewart and Oke (2012)], nor does it distinguish possible intra-urban patch variations of α, it can still provide a useful first approximation of the daytime influence of porous land cover and vegetation on Q_E. The

resulting derived mean peak hourly daytime $Q_{E(natural)}$ magnitudes for each season (winter $= 174.5\,\mathrm{W\,m^{-2}}$; equinox $= 322.1\,\mathrm{W\,m^{-2}}$; pre-monsoon $= 452.3\,\mathrm{W\,m^{-2}}$; monsoon $= 492.8\,\mathrm{W\,m^{-2}}$) exceed available mean peak hourly turbulent energy (i.e. maximum $Q^* - \mathrm{RES}$) in the summer months (pre-monsoon $= 322.2\,\mathrm{W\,m^{-2}}$; monsoon $= 306.2\,\mathrm{W\,m^{-2}}$; equinox $= 233.6\,\mathrm{W\,m^{-2}}$), and is approximately equal in the winter ($153.8\,\mathrm{W\,m^{-2}}$). Incidentally, the large pre-monsoon and monsoon $Q_{E(natural)}$ fluxes exceed the magnitude of mean peak Q_E directly measured over a riparian mesquite (*Prosopis velutina*) woodland along the San Pedro River in southeastern Arizona in similar seasons (Scott *et al.*, 2004).

The relatively high measured evapotranspiration originating over the small proportion of vegetated surfaces and open water (total ~15% of source area) suggests that a strong intra-urban enhancement of advective effect from evapotranspiration is present at least during the day, which could be linked to the patchiness of small, irrigated grass and tree surfaces in the study area. This differs from a regional-scale (i.e. urban *vs* 'rural') oasis effect that requires either several EC towers sited across different LULC in Phoenix or analysis of several large-scale remote sensed images of the entire urban area. The consistent upward Q_E and downward Q_H observed at night throughout most seasons suggests that a larger, regional-scale oasis effect may be present nocturnally, but we cannot infer this with only a single tower and its limited source area at WPHX. Micro-scale field experiments (Hagashima *et al.*, 2007), and flux measurements over small urban parks in Sacramento (Spronken-Smith *et al.*, 2000), have shown that vegetation patches of low spatial density have higher evapotranspiration potential (i.e. evapotranspiration rate per unit vegetated area) when compared to larger, more homogenous green spaces. This is due to leading edge or the 'clothes-line' effect (Rosenberg, 1974), where a lack of obstacles to both insolation and turbulent advection of drier air results in high observed rates of evapotranspiration over small isolated vegetated areas. While the higher evapotranspiration potential is expected given the patchiness of green spaces in WPHX, what is surprising is that this large micro-scale process occurring over small lawns and tree surfaces appears to consistently integrate to the scale of measurement (i.e. local scale), especially during daytime in the driest season of the year. This result appears to support the conclusion from Moriwaki and Kanda (2004), who noted that micro-scale (e.g. Chow and Brazel, 2012) or local-scale numerical climate models (e.g. Georgescu *et al.*, 2011), typically assumed a uniform evaporation rate for urban vegetation as per a homogenous forest, which may underestimate observed urban Q_E in certain seasonal and geographical contexts. We do note that further investigation through other observational platforms complementing the WPHX tower is required to fully assess this influence of enhancement of evapotranspiration through advection over different scales.

4. Conclusion

Through direct observations, we compiled and analysed ensemble SEB fluxes from a suburban neighbourhood in Phoenix, AZ for four distinct seasons; winter, equinox, pre-monsoon and monsoon, for the calendar year 2012. The majority of energy over the diurnal period is partitioned into the RES and Q_H terms, which reflects the study area's aridity and thermal properties. Distinct seasonal variations in SEB partitioning exist, with increasing importance of turbulent transfer of energy through convection when more radiation energy is available in the summer; although, a much greater proportion of turbulent energy is partitioned in the Q_H term compared to Q_E during the dry winter months. Derived magnitudes of urban β are also among the largest in the urban SEB flux literature. The transition in phase when ensemble hourly Q_H is greater than the urban storage term also occurs earlier in the pre-monsoon and monsoon *versus* the winter season. The influence of evapotranspiration is limited, given the xeric nature of the site, but there exists the possibility of a micro-scale oasis effect arising from the relatively small vegetated land cover under urban irrigation within the study area through leading-edge effects. Comparisons with SEB data from other cities in different climates reveal some similarities, such as a strong hysteresis between X and Λ that could facilitate model parameterization during clear-sky weather conditions. However, the high proportion of radiative forcing that is stored in the residual term at this site, especially in summer, is large even when compared to SEB data from other arid climate cities. This feature suggests that waste heat via residential cooling from air conditioning within the site would be an important factor when analysing its SEB fluxes. Further, the impact of the presumptive micro-scale oasis effect on observed local-scale latent heat fluxes should be considered in future model design and parameterization for cities with similar SEB profiles.

The seasonal variations in radiative and turbulent fluxes observed from the WPHX tower are important towards increasing the knowledge of physical urban climate processes in a large arid city, in which previous research has been under-represented (Grimmond and Christen, 2012). Future analysis on the SEB response under various meteorological scenarios (e.g. extreme heat events or the immediate period after storm events), or on comparisons of observed SEB data with several urban climate models, would greatly complement and build upon findings from this study. Lastly, this information gained from this research can also be applied towards public policy for cities, like Phoenix, that are vulnerable to several urban climate hazards, such as on investigating whether modifications of residential neighbourhoods with similar physical characteristics through increased evapotranspiration (from outdoor misters or increased surface green-space) and/or surface alterations to its aspect ratio or α could be effective in improving thermal comfort of its urban residents.

References

Adams DK, Comrie AC. 1997. The North American monsoon. *Bull. Am. Meteorol. Soc.* **78**: 2197–2213.

Arnfield AJ. 2003. Two decades of urban climate research: a review of turbulence, exchanges of energy and water, and the urban heat island. *Int. J. Climatol.* **23**: 1–26.

Asaeda T, Ca VT. 1993. The subsurface transport of heat and moisture and its effect on the environment: a numerical model. *Bound.-Layer Meteorol.* **65**: 159–178.

Aubinet M, Vesala T, Papale D (eds). 2012. *Eddy Covariance: A Practical Guide to Measurement and Data Analysis*. Springer: New York, NY.

Blonquist JM Jr, Bugbee B, Tanner BD. 2009. Evaluation of measurement accuracy and comparison of two new and three traditional net radiometers. *Agr. For. Meteorol.* **149**: 1709–1721.

Brazel AJ, Fernando HJS, Hunt JCR, Selover N, Hedquist BC, Pardyjak E. 2005. Evening transition observations in Phoenix, Arizona. *J. Appl. Meteorol.* **44**: 99–112.

Chow WTL, Brazel AJ. 2012. Assessing xeriscaping as a sustainable heat island mitigation approach for a desert city. *Build. Environ.* **47**: 170–181, DOI: 10.1016/j.buildenv.2011.07.027.

Chow WTL, Pope RL, Martin CA, Brazel AJ. 2011. Observing and modeling the nocturnal park cool island of an arid city: horizontal and vertical impacts. *Theor. Appl. Climatol.* **103**: 197–211, DOI: 10.1007/s00704-010-0293-8.

Chow WTL, Brennan D, Brazel AJ. 2012. Urban heat island research in Phoenix, Arizona: theoretical contributions and policy applications. *Bull. Am. Meteorol. Soc.* **93**(4): 517–530, DOI: 10.1175/BAMS-D-11-00011.1.

Christen A, Vogt R. 2004. Energy and radiation balance of a central European city. *Int. J. Climatol.* **24**: 1395–1421.

Christen A, Coops NC, Crawford BR, Kellett R, Liss KN, Olchovski I, Oke TR, van der Lann M, Voogt JA. 2011. Validation of modeled carbon dioxide emissions from an urban neighborhood with direct eddy-covariance measurements. *Atmos. Environ.* **45**(33): 6057–6069, DOI: 10.1016/j.atmosenv.2011.07.040.

Coutts AM, Beringer J, Tapper NJ. 2007. Impact of increasing urban density on local climate: spatial and temporal variations in the surface energy balance in Melbourne, Australia. *J. Appl. Meteorol. Climatol.* **46**: 477–493.

Doll D, Ching JKS, Kaneshiro J. 1985. Parameterisation of subsurface heating for soil and concrete using net radiation data. *Boundary-Layer Meteorology.* **32**: 351–372.

Ellefsen R. 1990/1991. Mapping and measuring buildings in the canopy boundary layer in ten US cities. *Energy and Buildings* **15–16**: 1025–1049.

Fernando HJS, Zajic D, Di Sabatino S, Dimitrova R, Hedquist B, Dallman A. 2010. Flow, turbulence, and pollutant dispersion in urban atmospheres. *Phys. Fluids* **22**(5): 051301, DOI: 10.1063/1.3407662.

Frey CM, Parlow E, Vogt R, Harhash M, Wahab MMA. 2011. Flux measurements in Cairo, part 1: *in situ* measurements and their applicability for comparison with satellite data. *Int. J. Climatol.* **31**: 218–231, DOI: 10.1002/joc.2140.

Garcia-Cueto R, Jauregui E, Tejeda A. 2003. Urban/rural energy balance observations in a desert city in northern Mexico. In *Proceedings Fifth International Conference on Urban Climate*, ICUC-5. Lodz, Poland, 1–5 September 2003 (Proceedings CD-ROM).

Georgescu M, Moustaoui M, Mahalov A, Dudhia J. 2011. An alternative explanation of the semiarid urban area "oasis effect". *J. Geophys. Res.* **116**: D24113, DOI: 10.1029/2011JD016720.

Gober P, Brazel AJ, Quay R, Myint S, Grossman-Clarke S, Miller A, Rossi S. 2010. Using watered landscapes to manipulate urban heat island effects: how much water would it take to cool Phoenix? *J. Am. Plann. Assoc.* **76**(1): 109–121, DOI: 10.1080/01944360903433113.

Grimmond CSB, Christen A. 2012. Flux measurements in urban ecosystems. *Fluxl. Newsl. Fluxnet* **5**(1): 1–8.

Grimmond CSB, Oke TR. 1995. Comparison of heat fluxes from summertime observations in the suburbs of four North American cities. *J. Appl. Meteorol.* **34**: 873–889.

Grimmond CSB, Oke TR. 1999. Aerodynamic properties of urban areas derived from analysis of surface form. *J. Appl. Meteorol.* **38**: 1262–1292.

Grimmond CSB, Oke TR. 2002. Turbulent heat fluxes in urban areas: observations and a local-scale urban meteorological parameterization scheme (LUMPS). *J. Appl. Meteorol.* **41**: 792–810.

Grimmond CSB, Salmond JA, Oke TR, Offerle B, Lemonsu A. 2004. Flux and turbulence measurements at a dense urban site in Marseille: heat, mass (water, carbon dioxide) and momentum. *J. Geophys. Res.* **109**(D24): D24101, DOI: 10.1029/2004JD004936.

Grimmond CSB, Blackett M, Best MJ, Barlow J, Baik J-J, Belcher SE, Bohnenstengel SI, Calmet I, Chen F, Dandou A, Fortuniak K, Gouvea ML, Hamdi R, Hendry M, Kawai T, Kawamoto Y, Kondo H, Krayenhoff ES, Lee S-H, Loridan T, Martilli A, Masson V, Miao S, Oleson K, Pigeon G, Porson A, Ryu Y-H, Salamanca F, Shashua-Bar L, Steeneveld G-J, Trombou M, Voogt J, Young D, Zhang N. 2010a. The international urban energy balance models comparison project: first results from phase 1. *J. Appl. Meteorol. Climatol.* **49**: 1268–1292, DOI: 10.1175/2010JAMC2354.1.

Grimmond CSB, Roth M, Oke TR, Au YC, Best M, Betts R, Carmichael G, Cleugh H, Dabberdt W, Emmanuel R, Freitas E, Fortuniak K, Hanna S, Klein P, Kalkstein LS, Liu CH, Nickson A, Pearlmutter D, Sailor D, Voogt J. 2010b. Climate and more sustainable cities: climate information for improved planning and management of cities (producers/capabilities perspective). *Proc. Environ. Sci.* **1**: 247–274, DOI: 10.1016/j.proenv.2010.09.016.

Grimmond CSB, Blackett M, Best MJ, Barlow J, Baik J-J, Belcher SE, Bohnenstengel SI, Calmet I, Chen F, Dandou A, Fortuniak K, Gouvea ML, Hamdi R, Hendry M, Kawai T, Kawamoto Y, Kondo H, Krayenhoff ES, Lee S-H, Loridan T, Martilli A, Masson V, Miao S, Oleson K, Pigeon G, Porson A, Ryu Y-H, Salamanca F, Shashua-Bar L, Steeneveld G-J, Trombou M, Voogt J, Young D, Zhang N. 2011. Initial results from Phase 2 of the international urban energy balance model comparison. *Int. J. Climatol.* **31**: 244–272, DOI: 10.1002/joc.2227.

Grossman-Clarke S, Zehnder JA, Stefanov WL, Liu Y, Zoldak MA. 2005. Urban modifications in a mesoscale meteorological model and the effects on near-surface variables in an arid metropolitan region. *J. Appl. Meteorol.* **44**: 1281–1297.

Guido Z. 2009. Understanding the southwestern monsoon. *Southwest Climate Change Network*: *Feature Article*. http://www.southwestclimatechange.org/feature-articles/southwest-monsoon.

Hagashima A, Narita K, Tanimoto J. 2007. Field experiment on transpiration from isolated urban plants. *Hydrol. Process.* **21**: 1217–1222, DOI: 10.1002/hyp.6681.

Jenerette GD, Harlan SL, Stefanov W, Martin CA. 2011. Ecosystem services and urban heat riskscape moderation: water, green spaces, and social inequality in Phoenix, USA. *Ecol. Appl.* **21**: 2637–2651.

Kaimal JC, Finnigan JJ. 1994. *Atmospheric Boundary Layer Flows – Their Structure and Measurement*. Oxford University Press: New York, NY.

Kljun N, Rotach MW, Schmid HP. 2002. A three-dimensional backward Lagrangian footprint model for a wide range of boundary layer stratifications. *Bound.-Layer Meteorol.* **103**: 205–226.

Kotthaus S, Grimmond CSB. 2012. Identification of micro-scale anthropogenic CO2, heat and moisture sources – processing eddy covariance fluxes for a dense urban environment. *Atmos. Environ.* **57**: 301–316, DOI: 10.1016/j.atmosenv.2012.04.024.

Lee TW, Lee JY, Wang ZH. 2012. Scaling of the urban heat island intensity using time-dependent energy balance. *Urban Clim.* , DOI: 10.1016/j.uclim.2012.10.005.

Loridan T, Grimmond CSB. 2012. Characterization of energy flux partitioning in urban environments: links with surface seasonal properties. *J. Appl. Meteorol. Climatol.* **51**: 219–241, DOI: 10.1175/JAMC-D-11-038.1.

Loridan T, Grimmond CSB, Offerle BD, Young DT, Smith T, Järvi L. 2011. Local-scale urban meteorological parameterization scheme (LUMPS): longwave radiation parameterization and seasonality related developments. *J. Appl. Meteorol. Climatol.* **50**: 185–202.

Middel A, Brazel AJ, Gober P, Myint SW, Chang H, Duh J-D. 2012a. Land cover, climate, and the summer surface energy balance in Phoenix, AZ, and Portland, OR. *Int. J. Climatol.* **32**(13): 2020–2032, DOI: 10.1002/joc.2408.

Middel A, Brazel AJ, Kaplan S, Myint SW. 2012b. Daytime cooling efficiency and diurnal energy balance in Phoenix, Arizona, USA. *Clim. Res.* **54**: 21–34, DOI: 10.3354/cr01103.

Mills G, Cleugh H, Emmanuel R, Endlicher EE, McGranahan G, Ng E, Nickson A, Rosenthal J, Steemer K. 2010. Climate information for improved planning and management of mega cities (needs perspective). *Proc. Environ. Sci.* **1**: 228–246, DOI: 10.1016/j.proenv.2010.09.015.

Moriwaki R, Kanda M. 2004. Seasonal and diurnal fluxes of radiation, heat, water vapor, and carbon dioxide over a suburban area. *J. Appl. Meteorol.* **43**: 1700–1710.

Myint SW, Gober P, Brazel A, Grossman-Clarke S, Weng Q. 2011. Per-pixel vs. object-based classification of urban land cover extraction using high spatial resolution imagery. *Remote Sens. Environ.* **115**: 1145–1161.

Newton T, Oke TR, Grimmond CSB, Roth M. 2007. The suburban energy balance in Miami, Florida. *Geogr. Ann. Ser. A Phys. Geogr.* **89A**(4): 331–347.

Offerle B, Grimmond CSB, Fortuniak K. 2005a. Heat storage and anthropogenic heat flux in relation to the energy balance of a central European city centre. *Int. J. Climatol.* **25**: 1405–1419.

Offerle B, Jonsson P, Eliasson I, Grimmond CSB. 2005b. Urban modification of the surface energy balance in the West African Sahel: Ouagadougou, Burkina Faso. *J. Clim.* **18**: 3983–3995.

Offerle B, Grimmond CSB, Fortuniak K, Pawlak W. 2006. Intraurban differences of surface energy fluxes in a central European city. *J. Appl. Meteorol. Climatol.* **45**: 125–136.

Oke TR. 1987. *Boundary Layer Climates*, 2nd edn. London, UK: Methuen.

Oke TR. 1988. The urban energy balance. *Progr. Phys. Geogr.* **12**: 471–508, DOI: 10.1177/030913338801200401.

Oke TR. 2006. Initial guidance to obtain representative meteorological observations at urban sites. IOM Report No. 81. WMO/TD-No.1250. http://www.wmo.int/pages/prog/www/IMOP/publications/IOM-81/IOM-81-UrbanMetObs.pdf.

Oke TR, Zeuner G, Jauregui E. 1992. The surface energy balance in Mexico City. *Atmos. Environ.* **26B**: 433–444.

Oke TR, Spronken-Smith RA, Jauregui E, Grimmond CSB. 1999. The energy balance of central Mexico City during the dry season. *Atmos. Environ.* **33**: 3919–3930.

Pataki DE, Boone CG, Hogue TS, Jenerette GD, McFadden J, Pincetl S. 2011. Socio-ecohydrology and the urban water challenge. *Ecohydrology* **4**: 341–347.

Pigeon G, Legain D, Durand P, Masson V. 2007. Anthropogenic heat release in an old European agglomeration (Toulouse, France). *Int. J. Climatol.* **27**: 1969–1981, DOI: 10.1002/joc.1530.

Quah AKL, Roth M. 2012. Diurnal and weekly variation of anthropogenic heat emissions in a tropical city, Singapore. *Atmos. Environ.* **46**: 92–103, DOI: 10.1016/j.atmosenv.2011.10.015.

Roberts SM, Oke TR, Grimmond CSB, Voogt JA. 2006. Comparison of four methods to estimate urban heat storage. *J. Appl. Meteorol. Climatol.* **45**: 1766–1781.

Rosenberg NJ. 1974. *Microclimate: The Biological Environment*. Wiley-Interscience: New York, NY; 178–182.

Rotach MW, Vogt R, Bernhofer C, Batchvarova E, Christen A, Clappier A, Feddersen B, Gryning S-E, Martucci G, Mayer H, Mitev V,

Oke TR, Parlow E, Richner H, Roth M, Roulet Y-A, Ruffieux D, Salmond JA, Schatzmann M, Voogt JA. 2005. BUBBLE – An urban boundary layer meteorology project. *Theor. Appl. Climatol.* **81**: 231–261, DOI: 10.1007/s00704-004-0117-9.

Roth M. 2007. Review of urban climate research in (sub)tropical regions. *Int. J. Climatol.* **31**: 1859–1873, DOI: 10.1002/joc.1591.

Sailor DJ. 2011. A review of methods for estimating anthropogenic heat and moisture emissions in the urban environment. *Int. J. Climatol.* **31**: 189–299, DOI: 10.1002/joc.2106.

Sailor DJ, Lu L. 2004. A top-down methodology for developing diurnal and seasonal anthropogenic heating profiles for urban areas. *Atmos. Environ.* **38**(17): 2737–2748, DOI: 10.1016/j.atmosenv.2004.01.034.

Schmid HP. 1994. Source areas for scalars and scalar fluxes. *Bound.-Layer Meteorol.* **67**: 293–318.

Schmid HP, Cleugh HA, Grimmond CSB, Oke TR. 1991. Spatial variability of energy fluxes in suburban terrain. *Bound.-Layer Meteorol.* **54**: 249–276.

Scott RL, Edwards EA, Shuttleworth WJ, Huxman TE, Watts C, Goodrich DC. 2004. Interannual and seasonal variation in fluxes of water and carbon dioxide from a riparian woodland ecosystem. *Agr. For. Meteorol.* **122**: 65–84.

Spronken-Smith RA. 2002. Comparison of summer- and winter-time suburban energy fluxes in Christchurch, New Zealand. *Int. J. Climatol.* **22**: 979–992.

Spronken-Smith RA, Oke TR, Lowry WP. 2000. Advection and the surface energy balance across an irrigated urban park. *Int. J. Climatol.* **20**: 1033–1047.

Spronken-Smith RA, Kossmann M, Zawar-Reza P. 2006. Where does all the energy go? Surface energy partitioning in suburban Christchurch under stable wintertime conditions. *Theor. Appl. Climatol.* **84**: 137–149.

Stewart ID, Oke TR. 2012. Local climate zones for urban temperature studies. *Bull. Am. Meteorol. Soc.* **93**: 1879–1900, DOI: 10.1175/BAMS-D-11-00019.1.

Tejeda-Martinez A, Jauregui E. 2005. Surface energy balance measurements in the Mexico City region: a review. *Atmosfera* **18**: 1–23.

U.S. Census Bureau. 2010. *United States Census: 2010*. http://2010.census.gov/2010census/.

Vesala T, Järvi L, Launiainen S, Sogachev A, Rannik Ü, Mammarella I, Siivola E, Keronen P, Rinne J, Riikonen A, Nikinmaa E. 2008. Surface–atmosphere interactions over complex urban terrain in Helsinki, Finland. *Tellus* **60B**: 188–199, DOI: 10.1111/j.1600-0889.2007.00312.

Vivoni ER, Moreno HA, Mascaro G, Rodriguez JC, Watts CJ, Garatuza-Payan J, Scott RL. 2008. Observed relation between evapotranspiration and soil moisture in the North American monsoon region. *Geophys. Res. Lett.* **35**: L22403, DOI: 10.1029/2008GL036001.

Webb E, Pearman G, Leuning R. 1980. Correction of the flux measurements for density effects due to heat and water vapour transfer. *Q. J. R. Meteorol. Soc.* **106**: 85–100.

Willmott CJ. 1982. Some comments on the evaluation of model performance. *Bull. Am. Meteorol. Soc.* **63**(11): 1309–1313.

Wilson K, Goldstein A, Falge E, Aubinet M, Baldocchi D, Berbigier P, Bernhofer C, Ceulemans R, Dolman H, Field C, Grelle A, Ibrom A, Law BE, Kowalski A, Meyers T, Moncrieff J, Monson R, Oechel W, Tenhunen J, Valentini R, Verma S. 2002. Energy balance closure at FLUXNET sites. *Agr. For. Meteorol.* **113**: 223–243.

Zhu W-X, Hope D, Gries C, Grimm NB. 2006. Soil characteristics and the accumulation of inorganic nitrogen in an arid urban ecosystem. *Ecosystems* **9**: 711–724.